J. Phys. B: At. Mol. Opt. Phys. **42** (2009) 165010 (17pp) doi:10.1088/0953-4075/42/16/165010

Excitation energies, radiative and autoionization rates, dielectronic satellite lines and dielectronic recombination rates for excited states of Mg-like W from Na-like W

U I Safronova[1], **A S Safronova**[1] **and P Beiersdorfer**[2]

[1] Physics Department, University of Nevada, Reno, NV 89557, USA
[2] Physics Division, Lawrence Livermore National Laboratory, Livermore, CA 94550, USA

E-mail: ulyanas@unr.edu

Received 29 April 2009, in final form 24 June 2009
Published 31 July 2009
Online at stacks.iop.org/JPhysB/42/165010

Abstract

Energy levels, radiative transition probabilities and autoionization rates for $1s^2 2s^2 2p^6 3l'nl$ ($n = 3$–13, $l \leqslant n-1$), $1s^2 2s^2 2p^6 4l'nl$ ($n = 4$–7, $l \leqslant n-1$) and $1s^2 2s^2 2p^5 3l'3l''nl$ ($n = 3$–4, $l \leqslant n-1$) states in Mg-like tungsten (W^{62+}) are calculated using the Hartree–Fock-relativistic method (COWAN code), the multiconfiguration relativistic Hebrew University Lawrence Atomic Code (HULLAC code) and the relativistic many-body perturbation theory method (RMBPT code). Autoionizing levels above the thresholds $1s^2 2s^2 2p^6 3l$ and $1s^2 2s^2 2p^6 4l$ are considered. Branching ratios relative to the first threshold and intensity factors are calculated for satellite lines, and dielectronic recombination (DR) rate coefficients are determined for the first excited odd- and even-parity states. It is shown that the contribution of the highly excited states is very important for the calculation of total DR rates. Contributions to DR rate coefficients from the excited $1s^2 2s^2 2p^6 3l'nl$ states with $n \geqslant 14$ and $1s^2 2s^2 2p^6 4l'nl$ states with $n \geqslant 8$ and additionally from core-excited $1s^2 2s^2 2p^5 3l'3l''nl$ states with $n \geqslant 5$ are estimated by extrapolation of all atomic parameters. The orbital angular momentum quantum number l distribution of the rate coefficients shows two peaks at $l = 2$ and $l = 5$. The total DR rate coefficient is derived as a function of electron temperature. The dielectronic satellite spectra of W^{62+} are important for L-shell diagnostic of very high-temperature laboratory plasmas such as future ITER plasmas.

(Some figures in this article are in colour only in the electronic version)

1. Introduction

There has been great renewed interest in the spectral emission of tungsten from magnetically confined high-temperature plasmas. Several tokamaks, including the Joint European Torus (JET) and ASDEX, have in recent years been outfitted with plasma-facing components made of tungsten or soon will be. These components provide a steady supply of tungsten, which enters the plasma edge after being sputtered at the wall and diffuses all the way to the core [1, 2]. The design of the large international ITER tokamak also foresees the use of tungsten, and tungsten ions are expected to be present in the plasma at a concentration of 10^{-6} –10^{-5} [3, 4]. The plasma temperature in ITER may be as high as 30 keV in the core, so that tungsten ions may assume near-neon-like charge states, i.e., W^{60+}–W^{66+}, and emit L-shell x-ray radiation. As a result, the radiation of tungsten ions has been studied in several recent publications both theoretically and experimentally, and several overviews of the existing effort and available data have been given [5–11].

In this paper, we focus on the radiation produced by Mg-like tungsten following dielectronic recombination (DR) of Na-like tungsten. These ionization states of tungsten are expected to exist in the core of future ITER plasmas, and the radiation from these ions may affect the spectral lines proposed for use in core ion temperature and core rotation measurements [12].

Numerous papers were devoted to the investigation of properties of Mg-like ions; however, only few papers have considered the properties of highly charged ions with nuclear charge $Z = 74$, W^{62+}. Recently, measurements and a detailed analysis of extreme ultraviolet (EUV) spectra (40–200 Å) of highly charged tungsten ions W^{54+}–W^{63+} obtained with an electron beam ion trap was presented by Ralchenko *et al* [13]. The calculated wavelengths and emissivities versus temperature of the brightest spectral lines expected to be emitted by the tungsten ions (W^{58+}–W^{71+}) at extreme ultraviolet wavelengths longer than 45 Å were presented by Feldman *et al* [14]. Only one line ($3s^2\ ^1S_0$–$3s3p\ ^3P_1$) of Mg-like W^{62+} was considered in [13, 14]. The energy levels and spectral lines of multiply ionized tungsten atoms, W^{2+} through W^{73+}, were recently compiled by Kramida and Shirai in [11]. A list of energy levels for W^{62+} includes only four values ($3s3p\ ^{1,3}P_J$) [11].

Energies and multipole transition rates between the $3s^2$ and $3s3p\ ^{1,3}P_J$ levels calculated using the multiconfiguration Dirac–Hartree–Fock (MCDF) approach were presented by Zou and Froese Fischer [15] for Mg-like W. The influence of the hyperfine interaction on the energy separation of the $3s3p\ ^{1,3}P_J$ levels as a function of nuclear spin I and nuclear charge Z was investigated by Marques *et al* [16]. Energies and lifetime values for the $3s3p\ ^{1,3}P_J$ levels evaluated by the MCDF approach (Desclaux's code) were given for Mg-like tungsten [16]. The relativistic random-phase approximation (RPA) was used in [17] to calculate the excitation energies and oscillator strengths for the $3s^2\ ^1S_0$–$3snp\ ^{1,3}P_1$ transition in Mg-like W. The paper by Carson *et al* [18] was probably one of the first publication concerning ionization potentials (IP) for highly charged ions (along with the IP = 6919 eV for the W^{62+} ion). The calculation was based on a simple spherical shell solution for neutral atoms. More than 30 years later, the Dirac–Fock approximation was used to evaluate the total atomic energies of ground-state configurations for the lithium (3 electrons) to the dubnium (105 electrons) isoelectronic series [19]. It was found that the ionization potential for the W^{62+} ion is 6997 eV.

Excitation energies ($3s3p\ ^{1,3}P_J$ and $3p^2\ ^3P_J$, $^1D_2$, $^1S_0$ levels) and line strengths for all dipole transitions were calculated by Cheng and Johnson [20] for Mg-like ions including the W^{62+} ion. The multiconfiguration Hartree–Fock technique was used in that calculations. Excitation energies of the $3l_13l_2$ states calculated in the model-potential relativistic perturbation theory approach were presented by Ivanova *et al* [21], and numerical results were given for Mg-like ions with nuclear charge $Z = 25$–84. Excitation energies, transition probabilities and lifetimes were calculated for Mg-like ions with nuclear charges Z ranging from 13 to 100 by Safronova *et al* [22, 23]. The $3l_13l_2$–$3l_33l_4$ electric dipole transitions were investigated by using relativistic many-body perturbation theory (RMBPT). Most of results for highly charged ions in [22, 23] were presented graphically only.

Mg-like ions play a major role in the determination of DR rate coefficients for excited states of Mg-like W from Na-like W. Relativistic calculations of the DR rate coefficient for Ne-like tungsten (W^{64+}) in the ground state $2s^22p^6$ were performed by Behar *et al* [24]. The DR contributions of the most important Na-like W^{63+} doubly excited configuration complexes, namely, $(2s2p)^73ln'l'$ ($n' = 3$–13) and $(2s2p)^74l4l'$, were calculated by level-by-level computations [24]. Level-by-level relativistic calculations of DR rate coefficients for Ni-, Cu- and Ar-like tungsten in the ground state were performed by Behar *et al* [25]. The most important low-lying inner-shell excited configuration complexes were taken into account, namely $(3p3d)^{15}4l4l'$ for Ni-like W, $(3p3d)^{15}4s4l4l'$ for Cu-like W, and finally $3s^23p^53d9l$, $3s3p^63d7l$, and $3s^23p^54l4l'$ for Ar-like W. These complexes give the dominant contributions to the total DR rate coefficients for $kT_e < 0.5$ keV, and are still expected to give major contributions at higher electron temperature [25]. Total DR rate coefficient for Ar-like tungsten was evaluated by Peleg *et al* [26]. *Ab initio* calculations of the total DR rate coefficient for Ar-like tungsten (W^{56+}) were performed using the relativistic Hebrew University Lawrence Atomic code (HULLAC) package based on the parametric potential method. The high efficiency of HULLAC compared to other codes enables us to perform extensive DR calculations for highly complex atomic systems such as Ar-like tungsten [26]. *Ab initio* calculations of the total DR rate coefficient of Ni-like tungsten (W^{46+}) in the ground state were performed using the HULLAC atomic code package [27]. The present level-by-level calculations included the DR contributions of all levels (over 17 000) in the Cu-like (W^{45+}) inner-shell excited configurations $3d^94ln'l'$ ($n' \leqslant 9$), $3p^53d^{10}4l'l'$ ($n' \leqslant 5$) and $3s3p^63d^{10}4l'l'$ ($n' \leqslant 5$) [27]. An *ab initio* calculation of the total DR rate coefficient from the ground state $3s^23p^63d^9(J = 5/2)$ of Co-like tungsten was performed recently employing the relativistic distorted-wave approximation with configuration interaction [28]. The DR contributions mainly came from the $3d^84ln'l'$ complex. The $3p^53d^{10}n'l'$, $3p^53d^94ln'l'$ and $3d^85ln'l'$ complex series also contribute significantly to the total DR rates at relatively high electron temperatures [28].

The above-mentioned calculations [24–28] have considered only the total recombination rate. The DR contribution to the population of the different ionic excited states of Ne-like tungsten was recently considered by Safronova *et al* [10]. In that paper, the state-selective DR rate coefficients to excited states of Na-like tungsten as well as the total DR rate coefficients as a function of electron temperature were calculated. The DR rate coefficients were determined by direct calculation of the $1s^22s^22p^53l'nl$, $1s^22s2p^63l'nl$ ($n = 3$–7, $l \leqslant n-1$) and $1s^22s^22p^54l'nl$, $1s^22s2p^64l'nl$ ($n = 4$–6, $l \leqslant n-1$) states in Na-like tungsten using the COWAN, HULLAC and RMBPT codes [10].

In the present paper, we present the state-selective DR rate coefficients to excited states of Mg-like tungsten as well

as the total DR rate coefficients as a function of electron temperature. Energy levels, radiative transition probabilities and autoionization rates for the $1s^22s^22p^63l'nl$ ($n = 3$–13, $l \leqslant n-1$), $1s^22s^22p^64l'nl$ ($n = 4$–7, $l \leqslant n-1$) and $1s^22s^22p^53l'3l''nl$ ($n = 3$–4, $l \leqslant n-1$) states in Mg-like tungsten (W^{62+}) are calculated by the three codes: COWAN, HULLAC and RMBPT. Contributions from the excited $1s^22s^22p^63l'nl$ states with $n \geqslant 14$, $1s^22s^22p^64l'nl$ states with $n \geqslant 8$ and $1s^22s^22p^53l'3l''nl$ core-excited states with $n \geqslant 5$ to DR rate coefficients are estimated by extrapolation of all atomic parameters. The present paper extends our efforts on the calculation of the low-temperature DR rates coefficients, which we previously determined for Ne-like tungsten [10], Be-like carbon, oxygen and neon [29–31], B-like carbon and oxygen [32–34], C-like carbon and oxygen [35, 36], and Mg-like Fe [37].

We omit the core $1s^22s^2$ from the configuration notation in the text below.

2. Energy levels, transition probabilities and autoionization rates

Detailed calculations of DR parameters should include the determination of such characteristics as energies, radiative transition probabilities and autoionization rates for atomic states in the recombined ion. Therefore, we calculated the energies, radiative and autoionization rates for the intermediate states $2p^63l'nl$ ($n = 3$–13, $l' \leqslant 2, l \leqslant n-1$), $2p^64l'nl$ ($n = 4$–7, $l' \leqslant 3, l \leqslant n-1$) and $2p^53l'3l''nl$ ($n = 3$–4, $l \leqslant n-1$) for Mg-like tungsten (W^{62+}). The complete list includes 214 $2p^63l'nl$ configurations, 80 $2p^64l'nl$ configurations and 30 $2p^53l'3l''nl$ configurations (for a total of 7414 levels). Due to computational issues, the calculation of the DR parameters involving $2p^64l'nl$ and $2p^53l'3l''nl$ states was performed by including the $2p^63l'nl$ states only with $n \leqslant 9$ and $n \leqslant 4$, respectively. The resulting list of levels included in the set of $2p^63l'nl$ configurations with $n = 3$–13 consists of 1090 even-parity and 1084 odd-parity states, which give rise to 198 474 transitions. The set of $2p^64l'nl$ ($n = 4$–7) and $2p^63l'nl$ ($n = 3$–9) configurations contains 1007 even-parity and 1032 odd-parity states, which give rise to 182 276 transitions. The set of $2p^53l'3l''nl$ ($n = 3$–4) and $2p^63l'nl$ ($n = 3$–4) configurations contains 2261 even-parity and 2200 odd-parity states. These lead to 179 698 transitions.

Our large scale calculations of atomic properties are based on three atomic computer codes: the multiconfiguration Hartree–Fock (MCHF) code developed by Cowan (in the following we will refer to it as the COWAN code) [38], the multiconfiguration relativistic Hebrew University Lawrence Livermore Atomic Code (the HULLAC code) [39], and the relativistic many-body perturbation theory code (the RMBPT code). The RMBPT method was described in detail in [40, 41]. These three codes allow us to check the accuracy of our calculations, and agreement between the results from each code provides confidence that our predictions are reliable.

We use the version of the COWAN code available in [42]. That version allows us to take into account a large number of configurations (up to 100 odd- and 100 even-parity configurations). The scaling of electrostatic integrals in the COWAN code allows us to correct for correlation effects and to obtain good agreement with experimental energies. We employed a single scaling factor (0.85) for all electrostatic integrals.

In the HULLAC code, the intermediate-coupling detailed level energies are calculated using the relativistic version of the parametric potential method, including configuration mixing. The autoionization rate coefficients are calculated in the distorted-wave approximation, implementing the highly efficient factorization-interpolation method.

The RMBPT code, including the Breit interaction, is used to evaluate energies and transition rates for multipole transitions. This method is based on the relativistic many-body perturbation theory, agrees with MCDF calculations in lowest order, includes all second-order correlation corrections, and includes corrections from negative energy states. First-order perturbation theory is used to obtain intermediate-coupling coefficients, and second-order RMBPT is used to determine the matrix elements. The RMBPT code is an *ab initio* code without the scaling of electrostatic integrals as used in the Cowan code and without any parametric potentials as employed in the HULLAC code.

The results of calculations are presented in tables 1–8. In table 1, energies for the 35 $2p^63l3l'$ excited states of Mg-like tungsten are given. We compare the results obtained using all three codes. The difference between the results is about 0.1–0.5%, except for some levels (see, for example, the $2p^63s3p\ ^3P_0$, $^3P_1$ levels) where the difference is as much as 1–2%. It should be noted that we list in this table both LS (left column) and jj (right column) coupling labels for each level. The LS labelling is taken from the COWAN code, while the jj labelling is from the RMBPT code. We include also in table 1 the leading mixing coefficients of states in the LS and jj coupling schemes evaluated by the COWAN and RMBPT codes, respectively. It can be seen from this table that the jj coupling is more suitable to produce the energies of the $2p^63l3l'$ excited states in Mg-like tungsten. In addition, we list in the sixth column of table 1 energy values taken from [21]. Those results were obtained by using the relativistic perturbation theory with a model potential (PT-MP) in the zero-order approximation [21]. One can see from table 1 that the PT-MP results differ from our three results by 1–2%. We have already mentioned that in the recent compilation by Kramida and Shirai [11] energy values were given only for four levels, i.e. for $E(3s3p\ ^{1,3}P_J) = 1124$, 1251.4, 4390 and 4390 in 1000 cm^{-1} units for the $^3P_0$, $^3P_1$, $^1P_1$ and $^3P_2$ levels, respectively. The first three values are in best agreement with our RMBPT values, while the fourth value (for the $^3P_2$ level) disagrees with all values given in table 1.

In table 2, the wavelengths λ (in Å) and radiative transition rates A_r (in units of s^{-1}) for the $2p^63s^2$–$2p^63s3p$, $2p^63s3p$–$2p^63p^2$, $2p^63s3p$–$2p^63s3d$, $2p^63s3d$–$2p^63p3d$, $2p^63p^2$–$2p^63p3d$ and $2p^63p3d$–$2p^63d^2$ transitions are presented. Both LS-allowed (triplet–triplet and singlet–singlet) and inter-combination (triplet–singlet) transitions are included here. Comparison of the theoretical data obtained using the RMBPT, HULLAC and COWAN codes is given in six columns of

Table 1. Energies (10^3 cm^{-1}) of the $2p^6 3l3l'$ excited states of Mg-like tungsten W^{62+}, calculated using RMBPT, HULLAC and COWAN codes. The PT-MP values are from [21]. Leading mixing coefficients of states in LS and jj coupling scheme are evaluated by COWAN and RMBPT codes, respectively. Designations: $2p^6 3l3l' = 3l3l'$.

Level		E (10^3 cm^{-1})				Level	
LS coupl	LS%	COWAN	RMBPT	HULLAC	PT–MP	jj%	jj coupl.
$3s^2\ ^1S_0$	99	0.000	0.000	0.000	0.000	99	$3s_{1/2}3s_{1/2}(0)$
$3s3p\ ^3P_0$	100	1149.816	1126.449	1136.079	1112.2	100	$3s_{1/2}3p_{1/2}(0)$
$3s3p\ ^3P_1$	72	1271.524	1252.154	1267.584	1242.1	99	$3s_{1/2}3p_{1/2}(1)$
$3s3p\ ^3P_2$	100	4125.356	4104.094	4109.447	4156.1	100	$3s_{1/2}3p_{3/2}(2)$
$3s3p\ ^1P_1$	72	4399.741	4402.930	4414.698	4455.2	99	$3s_{1/2}3p_{3/2}(1)$
$3p^2\ ^3P_0$	69	2706.827	2687.591	2721.583	2661.9	99	$3p_{1/2}3p_{1/2}(0)$
$3p^2\ ^1D_2$	53	5583.677	5535.299	5557.115	5581.2	81	$3p_{1/2}3p_{3/2}(2)$
$3p^2\ ^3P_1$	100	5585.086	5551.449	5572.679	5587.6	100	$3p_{1/2}3p_{3/2}(1)$
$3p^2\ ^3P_2$	64	8607.162	8587.871	8608.270	8691.9	99	$3p_{3/2}3p_{3/2}(2)$
$3p^2\ ^1S_0$	68	8743.883	8742.077	8760.103	8843.5	99	$3p_{3/2}3p_{3/2}(0)$
$3s3d\ ^3D_1$	100	5772.978	5826.700	5842.706	5893.4	100	$3s_{1/2}3d_{3/2}(1)$
$3s3d\ ^3D_2$	66	5862.612	5930.433	5954.313	6000.4	80	$3s_{1/2}3d_{3/2}(2)$
$3s3d\ ^3D_3$	100	6451.470	6497.864	6514.682	6602.1	100	$3s_{1/2}3d_{5/2}(3)$
$3s3d\ ^1D_2$	69	6551.650	6638.292	6656.792	6739.9	93	$3s_{1/2}3d_{5/2}(2)$
$3p3d\ ^3F_2$	75	7032.922	7040.920	7073.000	7097.9	100	$3p_{1/2}3d_{3/2}(2)$
$3p3d\ ^3D_1$	53	7268.523	7319.021	7355.779	7375.7	99	$3p_{1/2}3d_{3/2}(1)$
$3p3d\ ^3P_2$	46	7832.965	7864.742	7891.697	7950.6	100	$3p_{1/2}3d_{5/2}(2)$
$3p3d\ ^3F_3$	51	7860.956	7888.737	7923.446	7983.4	99	$3p_{1/2}3d_{5/2}(3)$
$3p3d\ ^3D_2$	51	10 089.709	10 123.675	10 148.690	10 242.4	99	$3p_{3/2}3d_{3/2}(2)$
$3p3d\ ^3P_0$	100	10 155.694	10 204.774	10 225.388	10 317.7	100	$3p_{3/2}3d_{3/2}(0)$
$3p3d\ ^3P_1$	59	10 168.492	10 208.975	10 235.181	10 327.3	99	$3p_{3/2}3d_{3/2}(1)$
$3p3d\ ^3F_3$	48	10 171.919	10 205.527	10 239.308	10 332.8	97	$3p_{3/2}3d_{3/2}(3)$
$3p3d\ ^3F_4$	100	10 675.321	10 703.303	10 725.535	10 858.3	100	$3p_{3/2}3d_{5/2}(4)$
$3p3d\ ^3P_2$	46	10 763.719	10 798.476	10 819.397	10 948.9	99	$3p_{3/2}3d_{5/2}(2)$
$3p3d\ ^3D_3$	61	10 913.152	10 948.353	10 978.314	11 104.0	98	$3p_{3/2}3d_{5/2}(3)$
$3p3d\ ^1P_1$	65	11 000.873	11 050.425	11 076.381	11 203.3	99	$3p_{3/2}3d_{5/2}(1)$
$3d^2\ ^3F_2$	73	11 655.640	11 764.712	11 801.741	11 900.9	99	$3d_{3/2}3d_{3/2}(2)$
$3d^2\ ^3P_0$	69	11 830.419	11 979.693	12 012.701	12 110.7	98	$3d_{3/2}3d_{3/2}(0)$
$3d^2\ ^3F_3$	100	12 301.781	12 403.203	12 432.187	12 570.9	100	$3d_{3/2}3d_{5/2}(3)$
$3d^2\ ^3P_2$	49	12 383.832	12 501.277	12 531.285	12 668.9	99	$3d_{3/2}3d_{5/2}(2)$
$3d^2\ ^1G_4$	71	12 411.383	12 518.342	12 560.665	12 699.2	99	$3d_{3/2}3d_{5/2}(4)$
$3d^2\ ^3P_1$	100	12 413.004	12 545.045	12 567.072	12 704.2	100	$3d_{3/2}3d_{5/2}(1)$
$3d^2\ ^3F_4$	71	13 012.810	13 114.392	13 146.237	13 318.8	99	$3d_{5/2}3d_{5/2}(4)$
$3d^2\ ^1D_2$	47	13 077.950	13 198.696	13 224.202	13 396.2	100	$3d_{5/2}3d_{5/2}(2)$
$3d^2\ ^1S_0$	69	13 265.374	13 431.171	13 452.476	13 622.5	98	$3d_{5/2}3d_{5/2}(0)$

table 2. Similar to table 1, we list the LS labels of the levels in the left column and the jj labels in the right column of table 2. The wavelength results are seen to agree with each other at the 0.1–1% level, while the radiative transition rates agree at the 10–50% level. The sole experimental wavelength value (79.91(2) Å) given in [13] for the $2p^6 3s^2\ ^1S_0$–$2p^6 3s3p\ ^3P_1$ transition is in better agreement with our RMBPT value than with the HULLAC and COWAN values (see first row in table 2). It is rather strange that the Flexible Atomic Code (FAC) [43]) values (λ = 79.904 Å and $A_r = 1.82[10]$ s^{-1}) given in [13] are also in better agreement with our RMBPT values than with the HULLAC values. It will be interesting to know why the FAC code [43] gives better results than the HULLAC code for such a system as Mg-like tungsten.

In table 3, the energies and sums of the weighted radiative transition rates $\left(\sum g A_r\right)$ for the $2p^6 3l4l'$ excited states of Mg-like W calculated by the RMBPT, HULLAC and COWAN codes are compared. There is very good agreement among the energies (0.02–0.3% difference), while the differences in the values of $\sum g A_r$ can be equal to 50–70% for some levels. Unfortunately, we did not find any published results concerning these $2p^6 3l4l'$ excited states in Mg-like W. As in tables 1 and 2, we list the LS labels of a given level in the left column and the jj labels in the right column of table 3.

In table 4, the results for the energies of the $2p^6 4l4l'$ states obtained by the three codes are compared in columns COWAN, RMBPT and HULLAC, respectively. Unfortunately, no experimental or other theoretical data for the $2p^6 4l4l'$ states were found. One can see from table 4 that the RMBPT values are larger than the COWAN values, and, vice versa, the RMBPT values are smaller than the HULLAC values. The typical difference between the RMBPT and COWAN energies is about 0.15%, while the difference between the RMBPT and HULLAC energies is about 0.04%.

The weighted autoionization rates (gA_a in s^{-1}) for the $2p^6 4l4l'$ excited states of Mg-like W below the first $2p^6 3s$

Table 2. Wavelengths (λ in Å) and transition rates (A_r in s^{-1}) for transitions between $2p^6 3l3l'$ states in W^{62+} ion, calculated using RMBPT, HULLAC and COWAN codes. Designations: $2p^6 3l3l' = 3l3l'$. Numbers in square brackets represent powers of 10.

Transitions		λ_{RMBPT}	λ_{HULLAC}	λ_{COWAN}	A_r^{RMBPT}	A_r^{HULLAC}	A_r^{COWAN}	Transitions	
$3s^2\ ^1S_0$	$3s3p\ ^3P_1$	79.86	78.89	78.73	1.80[10]	2.67[10]	2.14[10]	$3s_{1/2}3s_{1/2}(0)$	$3s_{1/2}3p_{1/2}(1)$
$3s3d\ ^3D_3$	$3p3d\ ^3P_2$	73.16	72.62	72.49	4.20[10]	4.33[10]	4.70[10]	$3s_{1/2}3d_{5/2}(3)$	$3p_{1/2}3d_{5/2}(2)$
$3s3d\ ^3D_3$	$3p3d\ ^3F_3$	71.90	70.98	71.13	2.52[10]	2.62[10]	2.82[10]	$3s_{1/2}3d_{5/2}(3)$	$3p_{1/2}3d_{5/2}(3)$
$3s3p\ ^3P_2$	$3p^2\ ^1D_2$	69.87	69.07	69.17	3.17[10]	3.61[10]	3.57[10]	$3s_{1/2}3p_{3/2}(2)$	$3s_{1/2}3d_{3/2}(2)$
$3p3d\ ^3D_3$	$3d^2\ ^3P_2$	64.39	64.39	67.34	4.16[09]	3.42[09]	4.13[09]	$3p_{3/2}3d_{5/2}(3)$	$3d_{5/2}3d_{5/2}(2)$
$3p3d\ ^3F_4$	$3d^2\ ^3F_3$	58.83	58.59	61.19	4.88[09]	4.88[09]	4.58[09]	$3p_{3/2}3d_{5/2}(4)$	$3d_{3/2}3d_{5/2}(3)$
$3p^2\ ^3P_1$	$3p3d\ ^3D_1$	56.57	56.08	59.68	1.59[10]	1.57[10]	1.37[10]	$3s_{1/2}3d_{3/2}(1)$	$3p_{1/2}3d_{3/2}(1)$
$3p3d\ ^3F_4$	$3d^2\ ^1G_4$	55.10	54.49	57.24	2.09[10]	2.14[10]	1.86[10]	$3p_{3/2}3d_{5/2}(4)$	$3d_{5/2}3d_{5/2}(4)$
$3p^2\ ^3P_1$	$3p3d\ ^3P_2$	43.23	43.12	44.62	2.08[11]	2.22[11]	1.94[11]	$3s_{1/2}3d_{3/2}(1)$	$3p_{1/2}3d_{5/2}(2)$
$3s3p\ ^3P_2$	$3s3d\ ^3D_3$	41.78	41.58	42.97	2.48[11]	2.52[11]	2.33[11]	$3s_{1/2}3p_{3/2}(2)$	$3s_{1/2}3d_{5/2}(3)$
$3p3d\ ^3F_4$	$3d^2\ ^3F_4$	41.48	41.31	42.61	1.18[11]	1.19[11]	1.13[11]	$3p_{3/2}3d_{5/2}(4)$	$3d_{3/2}3d_{5/2}(4)$
$3s3p\ ^3P_2$	$3s3d\ ^1D_2$	39.46	39.26	40.73	7.32[10]	7.89[10]	6.73[10]	$3s_{1/2}3p_{3/2}(2)$	$3p_{1/2}3p_{3/2}(2)$
$3s3d\ ^3D_3$	$3p3d\ ^3D_2$	27.58	27.52	27.50	3.10[09]	3.07[09]	2.73[09]	$3s_{1/2}3d_{5/2}(3)$	$3p_{3/2}3d_{3/2}(2)$
$3s3d\ ^3D_3$	$3p3d\ ^3F_3$	26.97	26.85	26.91	3.16[10]	3.20[10]	2.72[10]	$3s_{1/2}3d_{5/2}(3)$	$3p_{3/2}3d_{3/2}(3)$
$3s3d\ ^3D_3$	$3p3d\ ^3F_4$	23.78	23.75	23.69	1.62[12]	1.65[12]	1.65[12]	$3s_{1/2}3d_{5/2}(3)$	$3p_{3/2}3d_{5/2}(4)$
$3s3p\ ^3P_1$	$3p^2\ ^3P_1$	23.26	23.23	23.15	6.50[11]	5.90[11]	6.39[11]	$3s_{1/2}3p_{1/2}(1)$	$3s_{1/2}3d_{3/2}(1)$
$3s3d\ ^3D_3$	$3p3d\ ^3P_2$	23.25	23.23	23.20	4.31[11]	4.39[11]	4.33[11]	$3s_{1/2}3d_{5/2}(3)$	$3p_{3/2}3d_{5/2}(2)$
$3s^2\ ^1S_0$	$3s3p\ ^1P_1$	22.71	22.65	22.73	2.57[12]	3.28[12]	2.59[12]	$3s_{1/2}3s_{1/2}(0)$	$3s_{1/2}3p_{3/2}(1)$
$3s3p\ ^3P_0$	$3p^2\ ^3P_1$	22.60	22.54	22.52	1.20[12]	1.29[12]	1.27[12]	$3s_{1/2}3p_{1/2}(0)$	$3s_{1/2}3d_{3/2}(1)$
$3p^2\ ^3P_1$	$3p3d\ ^3D_2$	21.87	21.85	22.23	7.20[11]	7.85[11]	7.52[11]	$3s_{1/2}3d_{3/2}(1)$	$3p_{3/2}3d_{3/2}(2)$
$3s3p\ ^3P_1$	$3s3d\ ^3D_1$	21.86	21.86	22.21	5.03[11]	4.62[11]	5.30[11]	$3s_{1/2}3p_{1/2}(1)$	$3p_{1/2}3p_{3/2}(1)$
$3p^2\ ^1D_2$	$3p3d\ ^3D_2$	21.79	21.78	22.14	1.45[12]	1.55[12]	1.48[12]	$3s_{1/2}3d_{3/2}(2)$	$3p_{3/2}3d_{3/2}(2)$
$3p^2\ ^3P_1$	$3p3d\ ^3P_1$	21.47	21.45	21.85	1.32[12]	1.34[12]	1.26[12]	$3s_{1/2}3d_{3/2}(1)$	$3p_{3/2}3d_{3/2}(1)$
$3p^2\ ^1D_2$	$3p3d\ ^3F_3$	21.41	21.36	21.75	3.58[11]	3.79[11]	2.94[11]	$3s_{1/2}3d_{3/2}(2)$	$3p_{3/2}3d_{3/2}(3)$
$3s3p\ ^3P_1$	$3s3d\ ^3D_2$	21.38	21.34	21.69	2.73[12]	2.81[12]	2.82[12]	$3s_{1/2}3p_{1/2}(1)$	$3s_{1/2}3d_{5/2}(2)$
$3s3p\ ^3P_0$	$3s3d\ ^3D_1$	21.28	21.25	21.63	1.09[12]	1.16[12]	1.05[12]	$3s_{1/2}3p_{1/2}(0)$	$3p_{1/2}3p_{3/2}(1)$

Table 3. Energies (E in 10^3 cm^{-1}) and sums of weighted radiative transition rates ($\sum g A_r$ in s^{-1}) of the $2p^6 3l4l'$ excited states of Mg-like W calculated by the RMBPT, HULLAC and COWAN codes. Designations: $2p^6 3l4l' = 3l4l'$. Numbers in square brackets represent powers of 10.

Level	E (10^3 cm^{-1})			$\sum g A_r$ (s^{-1})		Level
COWAN	COWAN	RMBPT	HULLAC	COWAN	HULLAC	RMBPT
$3s4d\ ^3D_1$	28 221.172	28 258.189	28 275.011	3.50[14]	3.61[14]	$3p_{1/2}4p_{1/2}(1)$
$3p4p\ ^3P_1$	28 940.576	28 932.956	28 961.942	1.73[14]	1.89[14]	$3p_{1/2}4p_{3/2}(1)$
$3d4s\ ^3D_2$	31 642.821	31 709.996	31 737.850	3.27[14]	4.88[14]	$3p_{3/2}4p_{3/2}(2)$
$3p4p\ ^3P_2$	31 975.334	31 979.937	32 007.034	3.12[14]	3.18[14]	$3p_{3/2}4f_{5/2}(2)$
$3p4f\ ^3G_5$	33 287.284	33 300.145	33 329.996	2.66[15]	2.70[15]	$3p_{3/2}4f_{7/2}(5)$
$3d4d\ ^3F_3$	34 263.701	34 351.149	34 383.287	7.32[14]	4.55[14]	$3d_{5/2}4s_{1/2}(3)$
$3d4d\ ^3G_5$	34 929.862	35 012.549	35 044.367	1.02[15]	1.11[15]	$3d_{5/2}4d_{5/2}(5)$
$3s4p\ ^3P_2$	27 609.237	27 619.457	27 632.906	6.81[13]	6.06[13]	$3s_{1/2}4p_{3/2}(2)$
$3s4p\ ^1P_1$	27 655.303	27 669.012	27 685.514	2.29[14]	3.72[14]	$3p_{1/2}4s_{1/2}(1)$
$3s4f\ ^3F_4$	28 987.756	29 021.055	29 037.236	2.09[15]	2.96[15]	$3s_{1/2}4f_{7/2}(4)$
$3p4s\ ^3P_2$	30 165.147	30 166.779	30 185.574	2.16[14]	1.72[14]	$3p_{3/2}4s_{1/2}(2)$
$3p4s\ ^1P_1$	30 198.927	30 203.000	30 224.279	2.29[14]	2.23[14]	$3p_{3/2}4s_{1/2}(1)$
$3p4d\ ^3P_1$	32 545.145	32 565.687	32 592.703	4.46[14]	7.01[14]	$3p_{3/2}4d_{5/2}(1)$
$3d4p\ ^3P_2$	32 885.120	32 951.467	32 981.947	2.80[14]	3.37[14]	$3d_{3/2}4p_{3/2}(2)$
$3d4p\ ^3F_4$	34 088.387	34 148.496	34 178.419	4.80[14]	4.75[14]	$3d_{3/2}4f_{5/2}(4)$

threshold ($I = 56\,460\,000$ cm^{-1} [11]) are also presented in table 4. It should be noted that our calculated RMBPT value for the first $2p^6 3s$ threshold is equal to $I = 56\,467\,000$ cm^{-1}. It was found that the 14 even-parity states ($2p^6 4s^2$, $2p^6 4p^2$ and $2p^6 4s4d$) and 20 odd-parity states ($2p^6 4s4p$, $2p^6 4s4f$ and $2p^6 4p4d$) are located just above the first threshold and thus that they are not autoionizing at all. The large difference (factor of 2, for some cases) between the gA_a values given in the columns labelled COWAN and HULLAC can be explained by the different approaches used in the COWAN and HULLAC codes for calculating partly autoionized states. In the COWAN code, the values of gA_a were calculated for all $2p^6 4l4l'$ states; however, in the HULLAC code the non-autoionized $2p^6 4l4l'$ states were not taken into account.

A limited set of the $2p^5 3l3l'3l''$ core-excited states of Mg-like W are presented in table 5. Energies (10^3 cm^{-1}), the sums of the weighted radiative transition rates ($\sum g A_r$ in s^{-1}) and the weighted autoionization rates (gA_a in s^{-1}) calculated by the HULLAC and COWAN codes are compared. The labelling

Table 4. Energies (E in 10^3 cm^{-1}) and weighted autoionization rates (gA_a in s^{-1}) of the $2p^6 4l4l'$ excited states of Mg-like W calculated by the RMBPT, HULLAC and COWAN codes. Designations: $2p^6 4l4l' = 4l4l'$. Numbers in square brackets represent powers of 10.

Level COWAN	E (10^3 cm^{-1})			gA_a (s^{-1})		Level RMBPT
	COWAN	RMBPT	HULLAC	COWAN	HULLAC	
4p4f ^{3}D$_1$	56 707.002	56 756.148	56 779.930	1.14[11]	1.61[11]	$4d_{3/2}4d_{5/2}(1)$
4p4f ^{3}D$_3$	56 782.751	56 831.890	56 855.240	1.14[11]	1.38[11]	$4p_{3/2}4f_{5/2}(3)$
4f^2 ^{3}F$_2$	57 922.561	57 990.782	58 014.956	4.45[12]	4.22[12]	$4f_{5/2}4f_{5/2}(2)$
4f^2 ^{3}P$_0$	58 030.097	58 110.781	58 135.703	2.42[12]	3.92[12]	$4f_{5/2}4f_{5/2}(0)$
4f^2 ^{3}P$_2$	58 082.195	58 162.811	58 182.425	6.38[12]	6.16[12]	$4f_{5/2}4f_{7/2}(2)$
4f^2 ^{3}P$_2$	58 217.029	58 298.507	58 322.313	8.76[12]	7.98[12]	$4f_{7/2}4f_{7/2}(2)$
4f^2 ^{1}S$_0$	58 350.855	58 443.932	58 474.360	1.05[13]	1.68[13]	$4f_{7/2}4f_{7/2}(0)$
4p4d ^{1}P$_1$	56 413.673	56 478.172	56 497.325	6.17[13]	2.28[13]	$4p_{3/2}4d_{5/2}(1)$
4d4f ^{3}F$_2$	57 216.296	57 286.805	57 305.027	3.75[12]	1.30[12]	$4d_{3/2}4f_{5/2}(2)$
4d4f ^{3}P$_2$	57 409.706	57 488.956	57 510.634	8.72[11]	6.18[11]	$4d_{3/2}4f_{7/2}(2)$
4d4f ^{3}D$_2$	57 544.515	57 618.724	57 640.137	1.56[12]	7.04[11]	$4d_{5/2}4f_{5/2}(2)$
4d4f ^{3}P$_2$	57 677.837	57 757.340	57 779.686	6.31[11]	5.08[11]	$4d_{5/2}4f_{7/2}(2)$

Table 5. Energies (E in 10^3 cm^{-1}), sums of weighted radiative transition rates ($\sum gA_r$ in s^{-1}), and weighted autoionization rates (gA_a in s^{-1}) for the $2p^5 3l3l'3l''$ core-excited states of Mg-like W calculated by the HULLAC and COWAN codes. Numbers in square brackets represent powers of 10.

Level COWAN	E (10^3 cm^{-1})		$\sum gA_r$ (s^{-1})		gA_a (s^{-1})		Level HULLAC
	HULLAC	COWAN	HULLAC	COWAN	HULLAC	COWAN	
$2p^5 3s^2 3d(^2P)$ ^{3}P$_0$	71 813.612	71 552.077	1.00[14]	1.01[14]	3.02[14]	1.45[14]	3s23d0301..00
$2p^5 3s^2 3d(^2P)$ ^{3}P$_1$	72 022.765	71 747.341	5.68[14]	2.69[14]	2.11[14]	2.80[14]	3s23d0302..02
$2p^5 3s3p^2(^1D)$ ^{3}P$_0$	72 203.613	71 903.205	3.31[13]	3.03[13]	4.14[14]	2.40[14]	3s3p20307..00
$2p^5 3s^2 3d(^2P)$ ^{1}D$_2$	72 744.628	72 458.220	2.24[14]	4.44[14]	2.85[12]	3.60[12]	3s23d0102..04
$2p^5 3s3p^2(^3P)$ ^{1}S$_0$	74 834.834	74 610.440	5.23[12]	5.71[12]	1.95[12]	1.28[12]	3s3p20106..00
$2p^5 3p^2 3d(^3P)$ ^{5}D$_0^a$	77 406.109	77 153.170	1.70[14]	7.96[13]	1.60[11]	1.15[11]	3p23d090d..00
$2p^5 3p^2 3d(^1D)$ ^{3}P$_0^a$	77 760.547	77 430.604	8.74[12]	1.68[13]	1.70[12]	1.11[12]	3s3d20506..00
$2p^5 3p^2 3d(^3P)$ ^{3}D$_1^a$	78 444.703	78 152.947	2.11[14]	1.54[14]	8.08[10]	2.82[10]	3p23d0308..02
$2p^5 3s3d^2(^3F)$ ^{3}D$_2^a$	78 875.715	78 488.689	3.31[15]	5.82[15]	2.41[14]	3.26[14]	3s3d20202..04
$2p^5 3s3p^2(^3P)$ ^{5}D$_0$	79 869.829	79 707.413	1.36[12]	2.48[12]	2.29[14]	1.26[14]	3s3p20401..00
$2p^5 3p^2 3d(^1S)$ ^{3}P$_0$	80 634.382	80 358.609	1.59[13]	1.00[13]	4.18[10]	4.71[10]	3p23d0701..00
$2p^5 3p^2 3d(^3P)$ ^{3}D$_2^b$	80 968.298	80 632.931	4.19[14]	3.36[14]	3.29[11]	7.89[11]	3p23d0709..04
$2p^5 3s3p^2(^3P)$ ^{5}P$_1$	82 461.770	82 370.129	1.40[14]	9.90[13]	1.99[12]	4.66[12]	3s3p20201..02
$2p^5 3s3p^2(^3P)$ ^{3}D$_1^b$	82 866.427	82 738.596	1.46[15]	7.23[14]	1.32[13]	3.19[13]	3s3p20206..02
$2p^5 3s3p^2(^3P)$ ^{3}P$_0^a$	82 887.655	82 758.547	6.74[13]	7.28[13]	1.84[12]	8.72[11]	3s3p20205..00
$2p^5 3p^2 3d(^3P)$ ^{5}D$_0$	88 759.313	88 576.516	3.11[15]	1.37[15]	1.73[12]	3.75[12]	3p23d0807..00
$2p^5 3p^2 3d(^3P)$ ^{3}P$_0^a$	88 972.187	88 700.325	1.40[15]	1.13[15]	7.01[12]	9.26[12]	3p23d0801..00
$2p^5 3p^2 3d(^1D)$ ^{3}P$_0$	89 486.680	89 276.996	3.37[13]	4.60[13]	3.02[11]	2.51[11]	3p23d020b..00
$2p^5 3p^2 3d(^3P)$ ^{1}P$_1^a$	89 854.961	89 562.449	5.22[14]	8.28[14]	7.17[12]	1.24[13]	3p23d0201..02

of the states used in the COWAN code (left column) and in the HULLAC code (right column) are also given in table 5. The level's name in the HULLAC code has 12 characters: the first five are the name of the parent non-relativistic configuration given in the input file, the next two digits represent the specific relativistic sub-configuration, and the next two represent part of the recoupling scheme used. The last two are twice the total J value of the level. It can be seen from a comparison of the results given in columns labelled HULLAC and COWAN that the differences in the energies are about 0.1–0.5%, while the differences in the $\sum gA_r$ values and the gA_a values evaluated by the HULLAC and COWAN codes are about 50–90% for some cases. The gA_a values are obtained by including the first $2p^6 3s$ threshold only. It should be noted that we can input only one energy value for the free-electron wavefunction in the COWAN code when we evaluate the gA_a values of core-excited states. We studied the dependence of the gA_a values calculated with different input energies (2.72 and 5.74 keV). The difference is about a factor of 2–3 for some cases with small gA_a values. The gA_a values obtained by the HULLAC code is between the gA_a values obtained by the COWAN code within 2.72 keV and 5.74 keV for the free-electron wavefunction energies. Results given in the last column of table 5 are for the free-electron wavefunction of 5.74 keV.

Data for the transitions between the $2p^6 3ln_1l_1$ and $2p^6 3l'n_2l_2$ states as well as between the $2p^6 3ln_1l_1$ and $2p^6 4l'n_2l_2$ states are given in tables 6 and 7. It should be noted that we do not need all 198 474 transitions to calculate the DR rate coefficients to excited states but rather only the transitions from the excited states (states under the first threshold, $2p^6 3s$) to the autoionizing states (states above the first threshold, $2p^6 3s$). The $2p^6 3dnl$ states become autoionizing states at $n \geqslant 9$, the $2p^6 3pnl$ states at $n \geqslant 11$, and the $2p^6 3snl$ states do not autoionize at any value of n. Thus, we obtain 61 850 transitions

Table 6. Autoionization rates (A_a in s^{-1}) and excitation energies (E $_S$ in eV) of the $2p^6 3l_1 nl_1$ states as well as wavelengths (λ in Å), weighted radiative rates (gA_r in s^{-1}), intensity factors (Q_d in s^{-1}) and effective emission rate coefficients ($C_S^{\rm eff}$ in $cm^3\ s^{-1}$) for transitions between the $2p^6 3l'nl$ excited and the $2p^6 3l_1 nl_1$ autoionization states of Mg-like tungsten. Designations: $2p^6 3l'nl = 3l'nl$. The $C_S^{\rm eff}(j,i)$ values are given for $T_e = 10$ keV. Numbers in square brackets represent powers of 10.

Level lower	Level upper	A_a s^{-1}	ΣA_a s^{-1}	E_S eV	ΣgA_r s^{-1}	gA_r s^{-1}	λ Å	Q_d s^{-1}	$C_S^{\rm eff}$ $cm^3\ s^{-1}$
$3d^2\ ^2P_2$	$3d9f\ ^3D_3$	4.03[12]	4.03[12]	126.4	1.58[14]	8.06[13]	2.2528	1.22[13]	1.00[-15]
$3p4f\ ^3G_4$	$3p11g\ ^3H_5$	2.36[13]	2.36[13]	85.2	8.59[13]	1.82[13]	4.1777	1.37[13]	1.12[-15]
$3p5f\ ^3G_4$	$3p11g\ ^3H_5$	2.36[13]	2.36[13]	85.2	8.59[13]	1.58[13]	7.1382	1.19[13]	9.74[-16]
$3p6f\ ^3G_5$	$3p11g\ ^3H_6$	2.65[13]	2.65[13]	85.6	1.10[14]	1.46[13]	11.6476	1.11[13]	9.09[-16]
$3d6g\ ^3I_7$	$3d9h\ ^3K_8$	2.37[12]	2.37[12]	128.7	1.01[14]	3.88[13]	14.8103	1.10[13]	9.03[-16]
$3s11g\ ^3G_4$	$3p11g\ ^3H_5$	2.36[13]	2.36[13]	85.2	8.59[13]	1.75[13]	23.1415	1.32[13]	1.08[-15]
$3s12i\ ^3I_6$	$3p12i\ ^3K_7$	6.24[12]	6.24[12]	157.6	6.21[13]	2.43[13]	23.1410	1.46[13]	1.19[-15]
$3s13g\ ^3G_5$	$3p13g\ ^3H_6$	1.62[13]	2.16[13]	212.8	7.54[13]	2.16[13]	23.1423	1.28[13]	1.03[-15]
$3s13i\ ^3I_7$	$3p13i\ ^3K_8$	5.71[12]	7.62[12]	213.3	6.16[13]	2.78[13]	23.1399	1.41[13]	1.14[-15]
$3p3d\ ^3F_3$	$3d9d\ ^3G_4$	4.59[12]	4.59[12]	35.9	1.67[14]	8.09[13]	2.1467	1.61[13]	1.33[-15]
$3p4d\ ^3F_3$	$3p11f\ ^3G_4$	2.09[13]	2.09[13]	83.9	1.03[14]	2.21[13]	4.0629	1.43[13]	1.17[-15]
$3p5d\ ^3F_4$	$3p11f\ ^3G_5$	1.80[13]	1.80[13]	84.5	1.50[14]	1.76[13]	7.0444	1.00[13]	8.22[-16]
$3p6g\ ^3H_6$	$3p11h\ ^3I_7$	1.89[13]	1.89[13]	86.1	9.11[13]	1.45[13]	11.7175	1.10[13]	9.00[-16]
$3s11f\ ^3F_4$	$3p11f\ ^3G_5$	1.80[13]	1.80[13]	84.5	1.50[14]	1.95[13]	23.1430	1.11[13]	9.08[-16]
$3s12h\ ^3H_6$	$3p12h\ ^3I_7$	1.55[13]	1.55[13]	157.5	7.67[13]	2.61[13]	23.1410	1.96[13]	1.60[-15]
$3s12k\ ^3K_7$	$3p12k\ ^3L_8$	1.90[12]	1.90[12]	157.7	5.87[13]	2.84[13]	23.1414	1.01[13]	8.20[-16]
$3s13h\ ^3H_6$	$3p13h\ ^3I_7$	1.25[13]	1.66[13]	213.1	6.60[13]	2.45[13]	23.1396	1.45[13]	1.18[-15]
$3s13k\ ^3K_8$	$3p13k\ ^3L_9$	1.78[12]	2.37[12]	213.4	5.94[13]	3.16[13]	23.1408	1.02[13]	8.27[-16]

Table 7. Autoionization rates (A_a in s^{-1}) and excitation energies (E_S in eV) for the $2p^6 4l'nl$ states as well as wavelengths (λ in Å), weighted radiative rates (gA_r in s^{-1}), intensity factors (Q_d in s^{-1}) and effective emission rate coefficients ($C_S^{\rm eff}$ in $cm^3\ s^{-1}$) for transitions between the $2p^6 3l'nl$ excited and the $2p^6 4l'nl$ autoionization states of Mg-like tungsten. Designations: $2p^6 3l'nl = 3l'nl$, $2p^6 4l'nl = 4l'nl$. The $C_S^{\rm eff}(j,i)$ values are given for $T_e = 10$ keV. Numbers in square brackets represent powers of 10.

Level lower	Level upper	A_a s^{-1}	ΣA_a s^{-1}	E_S eV	ΣgA_r s^{-1}	gA_r s^{-1}	λ Å	Q_d s^{-1}	$C_S^{\rm eff}$ $cm^3\ s^{-1}$
$3d4d\ ^3F_4$	$4d4f\ ^1H_5$	3.05[13]	3.05[13]	156.8	3.86[15]	2.32[15]	4.4044	1.85[14]	1.51[-14]
$3d5d\ ^3F_4$	$4f5d\ ^3G_5$	2.50[13]	7.49[13]	1414.3	3.42[15]	2.00[15]	4.3919	1.29[14]	9.27[-15]
$3s4s\ ^3S_1$	$4s5p\ ^3P_2$	1.63[13]	4.88[13]	975.6	5.01[14]	1.35[14]	2.5959	1.47[13]	1.10[-15]
$3p4f\ ^3G_4$	$4d4f\ ^3H_5$	6.08[12]	6.08[12]	111.7	3.96[15]	1.12[15]	3.7009	1.86[13]	1.52[-15]
$3s5g\ ^1G_4$	$4p5g\ ^1F_3$	2.65[12]	7.95[12]	1298.3	3.53[14]	3.37[14]	3.5763	1.53[13]	1.11[-15]
$3p5f\ ^3F_2$	$4s5f\ ^3F_3$	2.28[13]	6.84[13]	1052.3	1.07[15]	1.05[14]	4.0307	1.09[13]	8.12[-16]
$3d5s\ ^3D_2$	$4f5s\ ^3F_3$	1.39[13]	4.18[13]	1231.1	1.95[15]	1.56[15]	4.2894	6.78[13]	4.96[-15]
$3s6g\ ^1G_4$	$4p6g\ ^1F_3$	2.05[12]	6.16[12]	1959.9	4.03[14]	3.30[14]	3.5757	1.06[13]	7.23[-16]
$3d5d\ ^3F_3$	$4f5d\ ^3D_3$	6.55[12]	1.97[13]	1397.1	2.10[15]	5.31[14]	4.2846	1.09[13]	7.82[-16]
$3p6h\ ^3I_6$	$4d6h\ ^3K_7$	3.40[12]	1.02[13]	2032.0	2.48[15]	1.82[15]	3.6738	3.53[13]	2.38[-15]
$3s7g\ ^1G_4$	$4p7g\ ^1F_3$	1.86[12]	5.59[12]	2360.0	3.52[14]	3.35[14]	3.5748	1.12[13]	7.30[-16]
$3d6d\ ^3G_4$	$4f6d\ ^3H_5$	7.04[12]	2.11[13]	2078.5	3.29[15]	2.53[15]	4.2831	5.56[13]	3.74[-15]
$3p7f\ ^3G_5$	$4s7f\ ^3F_4$	8.19[12]	2.46[13]	2134.4	8.10[14]	2.15[14]	4.5728	1.53[13]	1.03[-15]
$3d7g\ ^3H_5$	$4f7g\ ^3H_5$	4.46[12]	1.34[13]	2501.5	2.85[15]	1.14[15]	4.2806	1.87[13]	1.21[-15]
$3p4s\ ^3P_1$	$4s5d\ ^3D_2$	2.62[13]	7.87[13]	1011.5	6.80[14]	2.86[14]	2.6693	3.50[13]	2.61[-15]
$3s4f\ ^3F_3$	$4p4f\ ^3G_4$	9.55[12]	9.55[12]	25.2	2.75[15]	3.85[14]	3.6003	1.17[13]	9.66[-16]
$3p4d\ ^3P_2$	$4d^2\ ^3P_2$	8.70[12]	8.70[12]	58.9	1.28[15]	3.41[14]	3.6887	1.13[13]	9.26[-16]
$3d4p\ ^3D_1$	$4p5p\ ^3D_2$	9.31[12]	2.79[13]	1123.3	4.72[14]	1.68[14]	3.0023	1.28[13]	9.49[-16]
$3d4f\ ^3G_5$	$4f^2\ ^3H_6$	3.27[13]	4.36[13]	199.0	6.26[15]	4.07[15]	4.4106	2.53[14]	2.05[-14]
$3p5g\ ^1H_5$	$4d5g\ ^1I_6$	2.64[13]	7.92[13]	1400.8	2.15[15]	1.02[15]	4.0848	1.10[14]	7.92[-15]
$3d5f\ ^3G_3$	$4f5f\ ^3H_4$	6.28[12]	1.88[13]	1421.0	3.04[15]	1.58[15]	4.2870	2.79[13]	2.00[-15]
$3p6d\ ^3P_2$	$4s6d\ ^3D_3$	1.40[13]	4.20[13]	1713.4	7.01[14]	1.10[14]	4.0227	1.09[13]	7.57[-16]
$3p7s\ ^3P_1$	$4d7s\ ^3D_2$	3.55[12]	1.06[13]	2353.9	6.41[14]	5.73[14]	3.6759	1.46[13]	9.56[-16]
$3d6f\ ^3G_3$	$4f6f\ ^3H_4$	4.09[12]	1.23[13]	2090.6	2.65[15]	1.58[15]	4.2843	2.11[13]	1.42[-15]
$3p7d\ ^3F_4$	$4s7d\ ^3D_3$	9.31[12]	2.79[13]	2123.7	5.49[14]	1.71[14]	4.5725	1.49[13]	9.99[-16]
$3d7f\ ^3H_4$	$4f7f\ ^3H_4$	2.51[12]	7.53[12]	2494.8	8.58[14]	5.33[14]	4.2801	1.30[13]	8.39[-16]
$3d7h\ ^3K_7$	$4f7h\ ^3L_8$	1.37[12]	4.11[12]	2505.3	4.59[15]	4.02[15]	4.2783	2.01[13]	1.29[-15]
$4s4f\ ^3F_4$	$4s5g\ ^3G_5$	4.50[12]	1.35[13]	1072.3	1.52[15]	7.72[14]	9.9137	2.29[13]	1.70[-15]

from the excited even-parity states to the $2p^6 3lnl'$ autoionizing odd-parity states and 63 422 transitions from the excited odd-parity states to the $2p^6 3lnl'$ autoionizing even-parity states. In tables 6 and 7, the transitions with the largest intensity factor,

Table 8. Autoionization rates (A_a in s^{-1}) and excitation energies (E_S in eV) for the core-excited $2p^5 3l'3l''nl$ states as well as wavelengths (λ in Å), weighted radiative rates (gA_r in s^{-1}), intensity factors (Q_d in s^{-1}) and effective emission rate coefficients ($C_S^{\rm eff}$ in $cm^3\ s^{-1}$) for transitions between the $2p^6 3l'nl$ excited and the $2p^5 3l'3l''nl$ core-excited states of Mg-like tungsten. The upper indices are used in the second column to differentiate between atomic terms. The $C_S^{\rm eff}(j,i)$ values are given for $T_e = 10$ keV. Numbers in square brackets represent powers of 10.

Level lower	Level upper	A_a s^{-1}	ΣA_a s^{-1}	E_S eV	ΣgA_r s^{-1}	gA_r s^{-1}	λ Å	Q_d s^{-1}	$C_S^{\rm eff}$ $cm^3\ s^{-1}$
$2p^6 3s3d\ ^3D_2$	$2p^5 3s3d^2(^1G)\ ^3F_3$	2.48[14]	3.85[14]	2742.7	1.54[16]	1.42[16]	1.3755	1.36[15]	8.59[-14]
$2p^6 3s4d\ ^3D_2$	$2p^5 3s3d4d(^2P)\ ^3F_3^d$	2.19[14]	2.25[14]	5537.6	1.54[16]	1.48[16]	1.3716	1.34[15]	6.36[-14]
$2p^6 3s^2\ ^1S_0$	$2p^5 3s^2 3d(^2P)\ ^3D_1$	5.55[13]	9.72[13]	3318.7	4.65[15]	4.26[15]	1.2015	1.44[14]	8.54[-15]
$2p^6 3p^2\ ^3P_0$	$2p^5 3s3p^2(^3P)\ ^5D_1$	9.58[13]	1.49[14]	2886.1	2.49[14]	2.43[14]	1.2984	1.00[14]	6.22[-15]
$2p^6 3p^2\ ^1D_2$	$2p^5 3p^2 3d(^1D)\ ^3G_3^b$	1.70[13]	1.06[14]	3978.1	7.46[15]	7.19[15]	1.2052	1.04[14]	5.80[-15]
$2p^6 3s3d\ ^3D_1$	$2p^5 3s3d^2(^1G)\ ^3F_2$	1.30[14]	1.42[14]	2726.1	4.56[15]	4.07[15]	1.3760	5.01[14]	3.16[-14]
$2p^6 3s3d\ ^3D_3$	$2p^5 3s3d4d(^2P)\ ^3F_4^e$	7.42[13]	7.54[13]	5544.3	4.73[15]	3.46[15]	1.0557	4.26[14]	2.03[-14]
$2p^6 3d^2\ ^3P_2$	$2p^5 3s3d^2(^3P)\ ^3D_3^a$	9.00[13]	9.70[13]	2799.4	2.92[15]	5.78[14]	1.5164	1.01[14]	6.32[-15]
$2p^6 3s4s\ ^3S_1$	$2p^5 3s3p4p(^2P)\ ^3P_2^d$	9.98[13]	3.08[14]	5215.1	9.95[14]	7.44[14]	1.3753	1.46[14]	7.19[-15]
$2p^6 3p4p\ ^3D_1$	$2p^5 3p3d4p(^2P)\ ^3F_2^i$	2.57[13]	2.19[14]	5464.9	1.01[16]	9.55[15]	1.3724	1.10[14]	5.27[-15]
$2p^6 3s4d\ ^3D_2$	$2p^5 3s3d4d(^2P)\ ^3F_2^d$	2.08[14]	2.25[14]	5544.5	1.15[16]	3.30[15]	1.3706	2.73[14]	1.30[-14]
$2p^6 3s3p\ ^3P_0$	$2p^5 3s3p3d(^2P)\ ^3D_1^h$	8.65[13]	9.14[13]	2151.7	7.66[15]	7.46[15]	1.3762	2.44[14]	1.63[-14]
$2p^6 3s3p\ ^3P_1$	$2p^5 3s3p3d(^2P)\ ^3D_2^h$	1.30[14]	1.36[14]	2166.5	1.29[16]	1.26[16]	1.3762	6.02[14]	4.01[-14]
$2p^6 3s4p\ ^3P_1$	$2p^5 3s3d4p(^2P)\ ^3D_2^a$	3.99[13]	5.51[13]	5314.1	7.42[15]	7.19[15]	1.3715	1.87[14]	9.07[-15]
$2p^6 3s4p\ ^3P_1$	$2p^5 3p^2 4p(^3P)\ ^5S_2$	2.86[13]	3.99[13]	5315.0	4.41[15]	4.23[15]	1.3714	1.31[14]	6.39[-15]
$2p^6 3s4p\ ^1P_1$	$2p^5 3s3d4p(^2P)\ ^1D_2^e$	4.78[13]	8.59[13]	5456.9	1.15[15]	7.46[14]	1.3733	1.13[14]	5.41[-15]
$2p^6 3s4f\ ^3F_2$	$2p^5 3s3d4f(^2P)\ ^3G_3^d$	8.08[13]	8.72[13]	5633.9	1.59[16]	8.91[15]	1.3692	3.04[14]	1.43[-14]
$2p^6 3s4f\ ^3F_3$	$2p^5 3s3d4f(^2P)\ ^1G_4^b$	2.53[13]	3.13[13]	5629.0	7.91[15]	4.84[15]	1.3704	1.35[14]	6.35[-15]
$2p^6 3s4f\ ^1F_3$	$2p^5 3s3d4f(^2P)\ ^1G_4^d$	5.87[13]	6.58[13]	5646.9	1.90[16]	1.33[16]	1.3704	3.57[14]	1.68[-14]
$2p^6 3s4f\ ^1F_3$	$2p^5 3s3d4f(^2P)\ ^3H_4^e$	2.53[13]	6.63[13]	6941.7	1.30[16]	9.90[15]	1.1988	1.66[14]	6.86[-15]

Q_d, are presented as an example; these transitions will be discussed in the following section.

In the third column (labelled A_a) of tables 6 and 7, the autoionization rates relative to the first threshold, $2p^6 3s$, are given. The next column in tables 6 and 7 shows autoionization rates as a sum of A_a (labelled $\sum A_a$) calculated relative to the $2p^6 3l$ thresholds with $l = 0, 1, 2$. The column labelled E_S in tables 6 and 7 lists excitation energies E_S relative to the first threshold, $2p^6 3s$, in eV. The E_S energy for the second and third thresholds is 160 eV and 721 eV, respectively. It should be noted that the $2p^6 3p\ ^2P$ term has a large fine structure [$^2P_{1/2} - ^2P_{3/2}$] splitting of 373 eV [11]. As a result, we include separate $2p^6 3p\ ^2P_{1/2}$ and $2p^6 3p\ ^2P_{3/2}$ thresholds with energies of 160 eV and 533 eV, respectively. Of course, $\sum A_a$ is equal to A_a for $0 \leqslant E_S \leqslant 160$ eV.

Autoionization rates (A_a and ΣA_a) and excitation energies (E_S in eV) for the core-excited $2p^5 3l'3l''nl$ states are illustrated in table 8. The column with ΣA_a heading shows autoionization rates as a sum of A_a calculated relative to the $2p^6 nl$ thresholds with $nl = 3s, 3p, 3d, 4s, 4p, 4d, 4f$. It should be noted that the $2p^5 3l'3l''nl$ core-excited states are all autoionizing states. Taking into account transitions from the $2p^6 3lnl'$ excited even-parity states to the $2p^5 3l'3l''nl$ core-excited odd-parity states, we obtain the 71 826 transitions instead of the 179 698 complete sets of transitions mentioned previously. The sum of the weighted radiative rates (ΣgA_r), the weighted radiative rates (gA_r) and wavelengths (λ) are given in the sixth, seventh and eight columns of table 8, respectively.

3. Dielectronic satellite spectra

The DR process to the bound states of the Mg-like ion occurs as an electron capture by the Na-like ion to the autoionizing states of the Mg-like ion followed by the radiative decay to the singly excited bound states:

$$\begin{aligned} &W^{63+}(2p^6 3s) + e \\ &\quad \rightarrow W^{62+*}(2p^6 3l_1 nl_2 + 2p^6 4l_1 nl_2 + 2p^5 3l_1 3l_2 nl_3) \\ &\quad \rightarrow W^{62+*}(2p^6 3l_1' nl_2' + 2p^6 4l_1' 4l_2') + h\nu \\ &\quad \downarrow \\ &W^{63+}(2p^6 3l, 2p^6 4l) + e. \end{aligned} \tag{1}$$

The ground state of W^{63+}, $2p^6 3s$, is the initial state. The autoionizing states are divided for three types of states: the core-excited $2p^5 3l_1 3l_2 nl_3$ states, the $2p^6 3l_1 nl_2$ states (for $2p^6 3pnl_2$ when $n \geqslant 11$ and for $2p^6 3dnl_2$ when $n \geqslant 9$), the $2p^6 4l_1 nl_2$ ($n_2 \geqslant 4$) states, except the 14 even-parity states ($2p^6 4s^2$, $2p^6 4p^2$ and $2p^6 4s4d$) and 20 odd-parity states ($2p^6 4s4p$, $2p^6 4s4f$ and $2p^6 4p4d$).

During the DR process, the dielectronic satellite (DS) lines are emitted when the electron jumps from doubly excited autoionization states to singly excited bound states. Radiative transitions from the $2p^6 3pnl$ states to the $2p^6 3snl$ states and those from the $2p^6 4pnl$ states to the $2p^6 3snl$ states give rise to satellite lines of the 3p–3s and 4p–3s lines of the Na-like tungsten. There also exist DR satellite transitions from autoionizing states $2p^6 3dnl$ to $2p^6 3pn'l$ with change of the principal quantum number n. They appear in a shorter wavelength region. Radiative transitions from the core-excited $2p^5 3l_1 3l_2 n_3 l_3$ to the excited non-autoionizing $2p^6 3ln'l'$ states

give rise to satellite lines to the 2p–nl (n =3, 4) transitions in Na-like tungsten.

Branching ratios K and relative intensity factor Q_d of the DS lines are defined as (see, for example, [44])

$$K(i,i_0) = \frac{A_a(i,i_0)}{\sum_{i_0'} A_a(i,i_0') + \sum_k A_r(k,i)},$$
$$Q_d(j,i) = g(i)A_r(j,i)K(i,i_0). \quad (2)$$

Here j denotes the bound state, i is the autoionizing state, i_0 is the initial state (that is, the $2p^6 3s$ ground state of the Na-like ion), and i_0' is the possible final state for autoionization, e.g., $2p^6 3l$ and $2p^6 4l$. The $g(i)$ is the statistical weight of the autoionizing state i, $A_a(i,i_0)$ is the autoionization rate from i to i_0, and $A_r(j,i)$ is the radiative transition probability from i to j.

Assuming a Maxwellian distribution, the effective emission rate coefficient of the DS line is obtained (see, for example, [45]):

$$C_S^{\rm eff}(j,i) = 3.3\times10^{-24}\left(\frac{I_H}{kT_e}\right)^{3/2}\frac{Q_d(j,i)}{g_0}$$
$$\times\exp\left(-\frac{E_S(i)}{kT_e}\right)\ \text{photons cm}^3\ \text{s}^{-1}, \quad (3)$$

where I_H is the ionization potential of hydrogen, g_0 is the statistical weight of the initial state i_0, $E_S(i)$ is the excitation energy of the autoionizing state i relative to the $2p^6 3s$ threshold, and T_e is the electron temperature. For cases where $A_a \gg A_r$ the branching ratio $K(j,i)$ is about $\simeq 1$, and the relative intensity factor, Q_d, is roughly estimated as $Q_d(j,i) \approx g(i)A_r(j,i)$.

As already mentioned above, autoionization rates $A_a(i,i_0) = A_a(i,3s)$, the sum of autoionization rates $\sum A_a(i,i_0') = A_a(i,3s) + A_a(i,3p) + A_a(i,3d) + A_a(i,4s) + A_a(i,4p) + A_a(i,4d) + A_a(i,4f)$, and the excitation energies E_S for even- and odd-parity states are presented in columns 3, 4 and 5 of tables 6–8. Weighted radiative rates $g_i A_r(j,i)$, sums of weighted radiative rates $\sum_k g_i A_r(k,i)$, and wavelengths λ for dipole-allowed transitions are given in columns 7, 6 and 8 of tables 6–8, respectively. The last two columns list the relative intensity factors, $Q_d(j,i)$, and the effective emission rate coefficients, $C_S^{\rm eff}(j,i)$, defined by equation (3). The $C_S^{\rm eff}(j,i)$ values are given for $T_e = 10$ keV. The number of transitions listed in tables 6–8 is limited by the largest values of the relative intensity factors $Q_d(j,i)$, namely, $Q_d(j,i) > 1.0\times10^{14}$ s^{-1} for the $2p^6 3l_1 n_2 l_2$–$2p^5 3l_3 3l_4 n_5 l_5$ transitions. This leaves only 20 lines in table 8 out of total of more than 140 000 transitions. The largest value of $Q_d(j,i)$ gives the largest value of effective emission rate coefficients $C_S^{\rm eff}(j,i)$ when the ratio of E_S and kT_e is not very large.

Figure 1 shows examples of DS spectra with $kT_e = 10$ keV for the $2p^6 3lnl'$–$2p^6 3l_1 nl_2$ and $2p^6 3lnl'$–$2p^6 4l_1 nl_2$ transitions. In two panels, we include data for 3218 even-odd parity transitions and 3449 odd-even parity transitions. The effective emission rate coefficients, $C_S^{\rm eff}(j,i)$, and Gaussian profiles with the commonly used spectral resolution, $R \equiv \lambda/\Delta\lambda = 800$, are utilized to synthesize these spectra (see for detail, for example, [46]). The limited set of transitions includes transitions with $C_S^{\rm eff}(j,i) > 10^{-16}$ cm^3 s^{-1}. The synthetic spectrum of DS lines from the W^{62+} ion at $T_e = 10$ keV is divided into two parts: $\lambda = 1.85$–3.1 Å and $\lambda = 3.5$–4.8 Å. Below, in this section, we use the short designations nl instead of $2p^6 nl$, $3l'nl$ instead of $2p^6 3lnl$, $4l'nl$ instead of $2p^6 4l'nl$ and $2p3l3l'nl_1$ instead of $2p^5 3l3l'nl_1$.

The strongest lines shown on the left panel of figure 1 are due to the Rydberg transitions [$3p^2$–3p11d, 3p12d] (λ = 1.92–1.94 Å), [3p3d–3d9d, 3d10d, 3p11f, 3p12f, 3p13f] (λ = 1.98–2.16 Å) and [$3d^2$–3d9f] ($\lambda = 2.25$ Å). The strongest lines in the region of 2.58–3.06 Å are due to the 3p4s–4s5d, 3p4f–4f5d and 3d4s–4s5f, 4s6f transitions.

The intensity of lines shown on the right panel of figure 1 is larger by a factor of 10–20 than all other lines shown on the left panel of figure 1. Three lines with $C_S^{\rm eff}$ equal to 15–31 in units of 10^{-15} cm^3 s^{-1} are due to the 3d4d ^{3}F$_4$–4d4f ^{1}H$_5$ ($\lambda = 4.404$ Å), 3d4f ^{3}G$_5$–4f^2 ^{3}H$_6$ ($\lambda = 4.411$ Å) and 3d4f ^{3}G$_5$–4f^2 ^{1}I$_6$ ($\lambda = 4.425$ Å). The upper states of transitions with the largest value of $C_S^{\rm eff}$ shown in the right panel of figure 1 are mainly the $4f^2$, 4d4f and 4f5d states.

A large number of satellite lines to the 3s–3p transitions (3s11l–3p11l, 3s12l–3p12l, and 3s13l–3p13l with $l = g, h, k, i$) are responsible for the spectra in the very narrow region of λ = 23.1396–23.1434 Å. The strong contributions from the 3p5f–3p11g and 3p5f − 3p12g transitions are in the region of λ = 6.88–7.16 Å and from the 3p6f–3p11g and 3p6g–3p11h transitions are in the region of λ = 11.64–11.72 Å. The are also contributions from the transitions 3d7g–3d9h and 3p8l–3p11(l + 1) with $l = f, g, h$ to the region with $\lambda = 28.3$ Å, and $\lambda = 30.85$–31.08 Å, respectively. The strongest lines with largest values of λ = 131.05–131.67 Å are due to the 3p10l–3p11(l + 1) transitions with $l = g, h$.

Figure 2 shows examples of DS spectra for $T_e = 10$ keV generated by the $2p^6 3lnl'$–$2p^5 3l_1 3l_2 n_3 l_3$ transitions. In this figure, we include data for 1032 even-odd parity transitions and 862 odd-even parity transitions. The effective emission rate coefficients $C_S^{\rm eff}(j,i)$ and Gaussian profiles with spectral resolution $R \equiv \lambda/\Delta\lambda = 2000$ are used to synthesize these spectra (see for detail, for example, [46]). The limited set of the transitions includes transitions with $320 > C_S^{\rm eff}(j,i) > 0.1$ in units of 10^{-15} cm^3 s^{-1}. The synthetic spectrum of DS lines from the W^{62+} ion at $T_e = 10$ keV is divided into four spectral regions: $\lambda = 0.94$–1.09 Å , $\lambda = 1.17$–1.25 Å , $\lambda = 1.28$–1.38 Å and $\lambda = 1.38$–1.59 Å (figure 2). The higher spectral resolution is used to show more resolved spectral features that occupied the narrower spectral bands than in figure 1.

The strongest lines shown in the top right panel of figure 2 are due to the $2p^6 3s3p$–$2p^5 3s3p3d$, $2p^6 3s3d$–$2p^5 3s3d^2$ and $2p^6 3p^2$–$2p^5 3s3p^2$ transitions in the very narrow region of λ = 1.2026–1.2031 Å with $C_S^{\rm eff}$ equal to 34–119 in units of 10^{-15} cm^3 s^{-1}. Those lines are the satellite lines to the $2p_{1/2}$–$3d_{3/2}$ resonance line at $\lambda = 1.2019$ Å of Ne-like tungsten (see, for example, [10]). We note one other strong line with $C_S^{\rm eff}$ equal to 45.5 in units of 10^{-15} cm^3 s^{-1}. It is identified as the $2p^6 3s^2$–$2p^5 3s3p^2$ transition. This line is caused by the mixing of the $2p^5 3s3p^2$ states with the $2p^5 3s^2 3d$ states.

The strongest lines shown in the bottom left panel of figure 2 are due to the $2p^6 3s3p$–$2p^5 3s3p3d$, $2p^6 3s3d$–$2p^5 3s3d^2$ and $2p^6 3p^2$–$2p^5 3s3p^2$ transitions. They are displayed in the

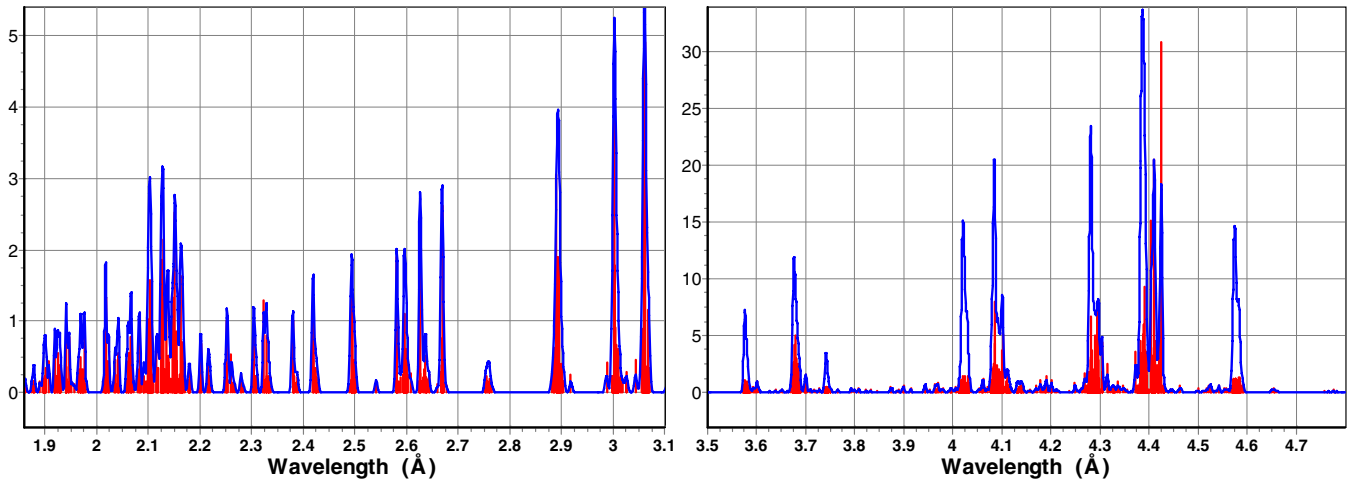

Figure 1. Synthetic spectra (red) of dielectronic satellite (DS) lines ($2p^6 3lnl'$–$2p^6 3l_1nl_2$ and $2p^6 3lnl'$–$2p^6 4l_1nl_2$) from the W^{62+} ion at $T_e =$ 10 keV for $\lambda = 1.85$–4.8 Å. Resolution $R = \lambda/\Delta\lambda = 800$ is assumed to produce a convoluted (Gaussian) profile (blue). The ordinate scale is the effective emission rate coefficients $C_S^{\rm eff}(j,i)$ in units of 10^{-15} cm^{3}s^{-1}.

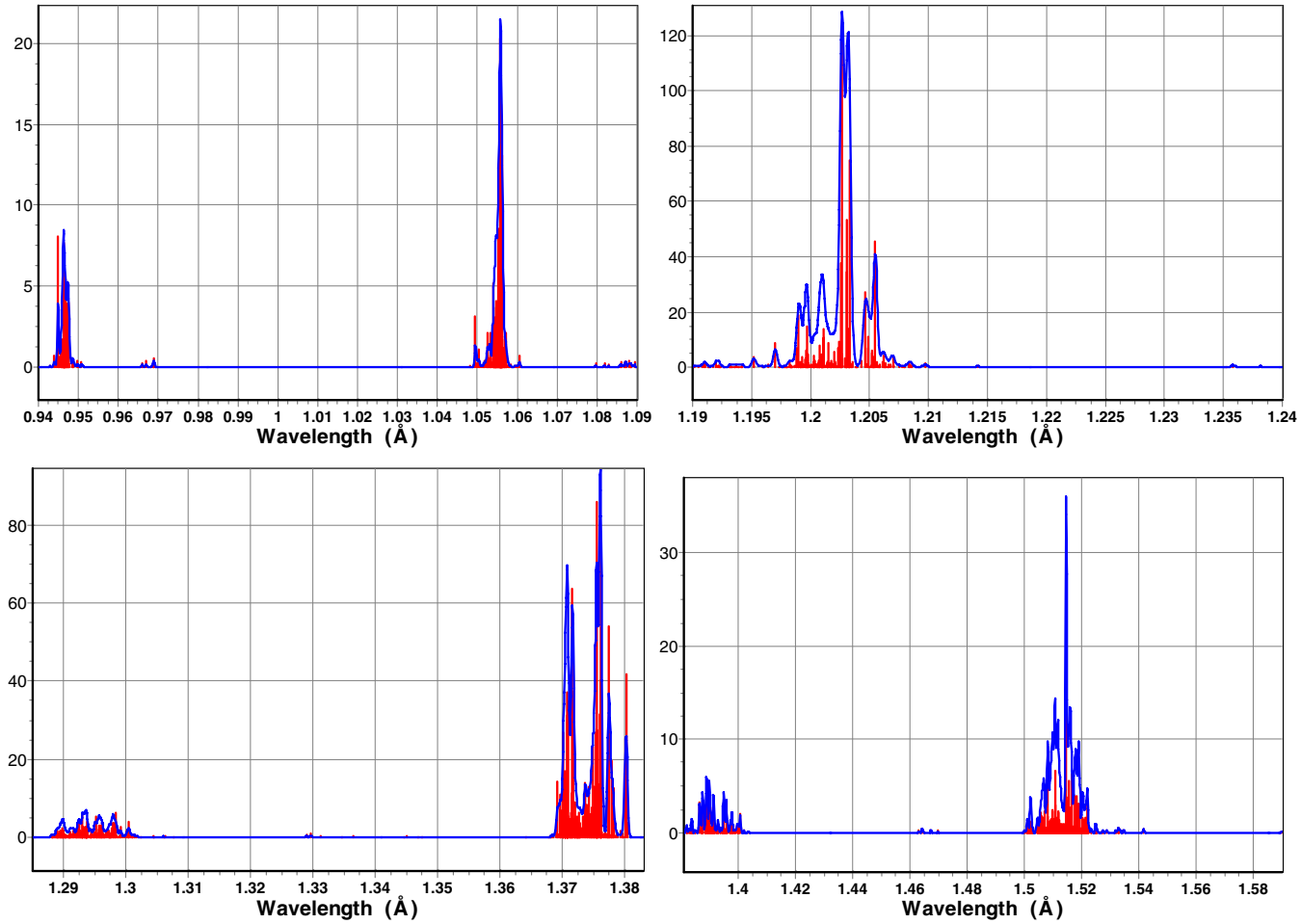

Figure 2. Synthetic spectra (red) of DS lines ($2p^6 3lnl'$–$2p^5 3l_1 3l_2 n_3 l_3$) from the W^{62+} ion at $T_e = 10$ keV for $\lambda = 0.9$–1.6 Å. A resolving power, $R = \lambda/\Delta\lambda = 2000$ is assumed to produce a Gaussian profile (blue). The scale in the ordinate is the effective emission rate coefficients $C_S^{\rm eff}(j,i)$ in units of 10^{-15} cm^{3}s^{-1}.

very narrow spectral region of $\lambda = 1.3755$–1.3762 Å with $C_S^{\rm eff}$ equal to 20–85 in units of 10^{-15} cm^3 s^{-1}. Those lines should be the satellite lines to the $2p_{3/2}$–$3d_{3/2}$ resonance lines at $\lambda =$ 1.3786 Å of Ne-like tungsten.

The satellite lines to the 2p–3s transition in Ne-like tungsten (at $\lambda = 1.4927$ Å) are displayed in the bottom right panel of figure 2. The strongest satellite lines are due to the $2p^6 3s3p$–$2p^5 3s^2 3p$, $2p^6 3p^2$–$2p^5 3s3p^2$ and $2p^6 3p3d$–$2p^5 3s3p3d$

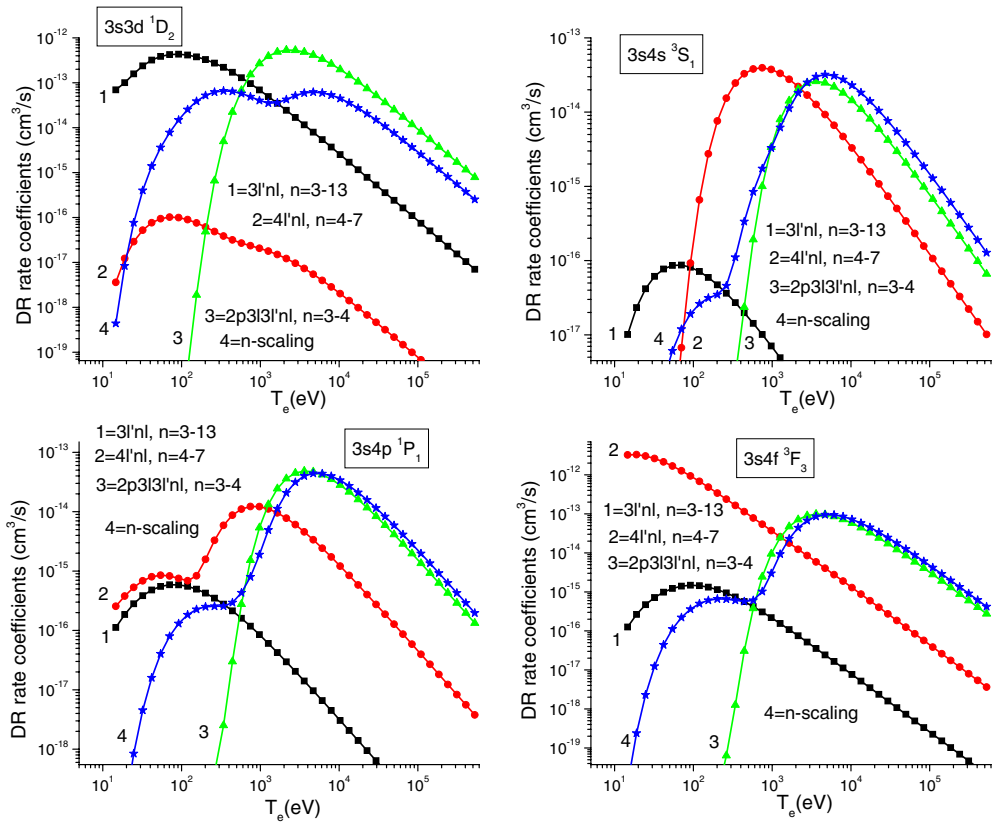

Figure 3. Contribution from the $2p^63lnl'$, $2p^64lnl'$, and $2p^53l3l'nl_1$ states to the DR rate coefficient $\alpha_d(3s, j)$ with $j = 3s3d\,^1D_2$, $3s4s\,^3S_1$, $3s4p\,^1P_1$ and $3s4f\,^3F_3$ as a function of T_e in Mg-like W. Curve 4 represents the sum of scaled contributions from the $2p^63lnl'$ states with $n = 14$–1000, from the $2p^64lnl'$ states with $n = 8$–1000, and from the $2p^53l3l'nl_1$ states with $n = 5$–1000.

transitions in the spectral region of $\lambda = 1.5080$–1.5145 Å with $C_S^{\rm eff}$ equal to 5–30 in units of 10^{-15} cm^3 s^{-1}.

The satellite lines to the 2p–4d transition in Ne-like tungsten (at $\lambda = 1.0416$ Å) are displayed in the top left panel of figure 2. The strongest satellite lines are due to the $2p^63s3p$–$2p^53s3p4d$ and $2p^63s3d$–$2p^53s3d4d$ transitions in the very narrow spectral region of $\lambda = 1.0552$–1.0563 Å with $C_S^{\rm eff}$ equal to 5–20 in units of 10^{-15} cm^3 s^{-1}.

4. Dielectronic recombination rate coefficients for excited states

The DR rate coefficients for excited states are obtained by summation of the effective emission rate coefficients $C_S^{\rm eff}(j, i)$ (equation (3)) for DR processes through all possible intermediate doubly excited states:

$$\alpha_d(i_0, j) = \sum_i C_S^{\rm eff}(j, i). \qquad (4)$$

For the DR process described by equation (1), we need to calculate $\alpha_d(i_0, j)$ with $i_0 = 2p^63s$ and all possible excited states j of W^{62+} with energies below the first threshold, $2p^63s$ (56 460 000 cm^{-1}). Among the $2p^63l'nl$, ($n = 3$–13), $2p^63pnl$, ($n = 3$–10) and $2p^63dnl$, ($n = 3$–8) states, 666 states of odd parity and 669 states of even parity have energies lower than 56 460 000 cm^{-1}. Among the $2p^64l'nl$ states, there are also 14 even-parity states ($2p^64s^2$, $2p^64p^2$ and $2p^64s4d$) and 20 odd-parity states ($2p^64s4p$, $2p^64s4f$ and $2p^64p4d$) with energies lower than 56 460 000 cm^{-1}. The sum over i includes the autoionizing $2p^63pnl$ states with $n \geqslant 11$, $2p^63dnl$ states with $n \geqslant 9$ and $2p^64l'nl$ states with $n \geqslant 4$ (except the 34 states mentioned above), and all core-excited $2p^53l'3l''nl$ states. Below, in this section, the short designations nl instead of $2p^6nl$, $3l'nl$ instead of $2p^63l'nl$, $4l'nl$ instead of $2p^64l'nl$ and $2p3l'3l''nl$ instead of $2p^53l'3l''nl$ are used.

In figure 3, we illustrate the contributions to $\alpha_d(3s, j)$ for some of j's from the sum over i with $n = 3$–13 (for autoionizing $3l'nl$ states), $n = 4$–7 (for autoionizing $4l'nl'$ states) and $n = 3$–4, (for core-excited $2p^53l'3l''nl$ states). Those contributions are represented by curves 1, 2 and 3, respectively. In figure 3, we show $\alpha_d(3s, j)$ with $j = 3s3d\,^1D_2$, $3s4s\,^3S_1$, $3s4p\,^1P_1$ and $3s4f\,^3F_3$. One can see that curve 1 is above curve 2 for the $3p3d\,^1D_2$ level, while curve 1 is under curve 2 for the $3s4p\,^1P_1$ and $3s4f\,^3F_3$ levels. For the $3s4s\,^3s_1$ level, the contributions of the $3lnl'$ autoionizing states are more important at low temperatures (15–70 eV) than the contributions of the $4lnl'$ autoionizing states, while at higher temperatures their relative contributions are opposite. The contributions of the $2p^53l'3l''nl$ states (curve 3) are more important for very high temperature T_e. Curve 3 is above curves 1 and 2 starting from T_e equal to 2 keV for all panels shown in figure 3. It is clearly seen that the contributions of the $3l'nl$, $4l'nl$ and $2p^53l'3l''nl$ states in the sum over i in equation (4) change with temperature, and all three types of states are important for the calculation of $\alpha_d(3s, j)$ for different values of j.

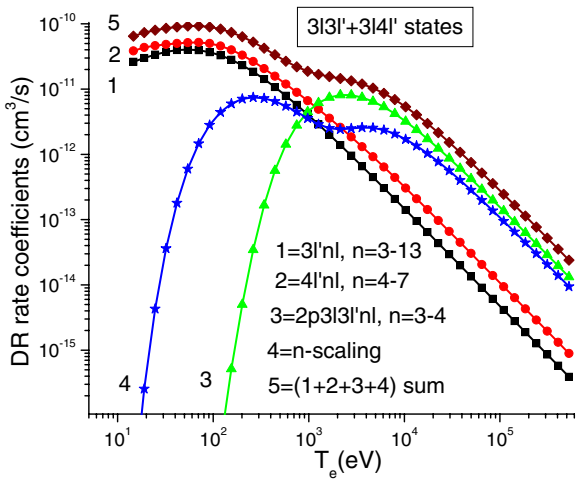

Figure 4. Contribution from the $2p^6 3lnl'$, $2p^6 4lnl'$ and $2p^5 3l3l'nl_1$ states to the DR rate coefficient, $\sum_j \alpha_d(3s, j)$, (where the summation over j includes the 35 $2p^6 3l3l'\,^{1,3}L_J$ and the 106 $2p^6 3l4l''\,^{1,3}L_J$ terms) as a function of T_e in Mg-like W. Curve 4 represents the sum of the scaled contribution from the $2p^6 3lnl'$ states with $n = 14$–1000, from the $2p^6 4lnl'$ states with $n = 8$–1000, and from the $2p^5 3l3l'nl_1$ states with $n = 5$–1000.

In order to estimate contributions from the high-n autoionizing states to the DR rate coefficients for excited states (sum over i with $n > 13$ for autoionizing $2p^6 3l'nl$ states, sum over i with $n > 7$ for autoionizing $2p^6 4l'nl$ states and sum over i with $n > 4$ for core-excited $2p^5 3l'3l''nl$ states), we use empirical scaling laws [35], which can only be implemented to include the one-electron 3s–np, 3p – ns, 3p – nd, 3d – np, 3d – nf, 2p – ns and 2p – nd dipole transitions. Additional contributions from the high-n states appear for the first low-lying configurations $3l3l'$ and $3l4l'$. For these configurations the [3s3p–3pnp], [3s3d–3dnp], [3p3d–3pnp, 3pnf, 3dns, 3dnd], [3p^2–3pns, 3pnd] and [3d^2–3dnp, 3dnf] transitions with $n > 13$ are to be included as well. Transitions with $n > 7$ are taken into account for the $3l4l'$ configurations: [3s4s–4snp], [3s4p–4pnp], [3s4f–4fnp], [3p4s–4sns, 4snd], [3p4p–4pns, 4pnd], [3p4d–4dns, 4dnd], [3p4f–4fns, 4fnd], [3d4s–4snp, 4snf], [3d4p–4pnp, 4pnf], [3d4d–4dnp, 4dnf] and [3d4f–4fnp, 4fnf]. Transitions with $n > 4$ core-excited states are taken into account for the $2p^6 3l3l'$ configurations: [$2p^6 3s3l'$–$2p^5 3s3l'ns$] and $2p^6 3s3l'$–$2p^5 3s3l'n$d]. Scaling contributions for a the $2p^6 3l4l'$ configurations from the core-excited $2p^5 3l'3l''nl$ states with $n > 4$ are due to the mixing of the [$2p^6 3l3l'$ + $2p^6 3l4l'$] configurations.

To estimate $Q_d(j, i)$ in equation (2) for autoionizing states i with the high principal quantum number n for the $3lnl'$ states and for the 3s–np, 3p–ns, nd, and 3d–np, nf dipole transitions, we used our calculated data for $n = 12$ and the $1/n^3$ scaling law for the rates A_a and A_r. For example, the formulae for the 3s3p–3pnp case are

$$A_a(3pnl^{1,3}L_J) = \left(\frac{12}{n}\right)^3 A_a(3p12l^{1,3}L_J), \tag{5}$$

$$A_r(3s3p\,^{1,3}P_{J'} - 3pnl^{1,3}L_J)$$

$$= \left(\frac{12}{n}\right)^3 A_r(3s3p\,^{1,3}P_{J'} - 3p12l^{1,3}L_J)$$

$$\times \left(\frac{\Delta E(3s3p\,^{1,3}P_{J'} - 3pnl^{1,3}L_J)}{\Delta E(3s3p\,^{1,3}P_{J'} - 3p12l^{1,3}L_J)}\right)^3. \tag{6}$$

In order to obtain the energies of the $3pnl^{1,3}L_J$ states as a function of nl, the following asymptotic formula was proposed in [37]:

$$E(3pnl) - E(3p) = -\frac{1}{2n^2}\left(Z - 11 + \frac{b(l)}{n}\right)^2, \tag{7}$$

where $b(s) = 2.873$, $b(p) = 1.761$, $b(d) = 0.721$, $b(f) = 0.137$, and $b(g) = 0.010$. The energy differences in equation (7) can be found by using the following formula:

$$\Delta E\left(3s3p\,^{1,3}P_{J'} - 3pnl^{1,3}L_J\right)$$

$$= \Delta E(3s3p\,^{1,3}P_{J'} - 3p12l^{1,3}L_J) - \frac{3969}{2}\left(\frac{1}{n^2} - \frac{1}{12^2}\right). \tag{8}$$

A similar formula was used for the excitation energies $E_S(i)$ in equation (3) when $i = 3pnl^{1,3}L_J$:

$$E_S(3pnl^{1,3}L_J) = E_S(3p12l^{1,3}L_J) - \frac{3969}{2}\left(\frac{1}{n^2} - \frac{1}{12^2}\right). \tag{9}$$

Using these scaling formulas for $A_a(3pnl^{1,3}L_J)$ and $A_r\left(3s3p\,^{1,3}P_{J'} - 3pnl^{1,3}L_J\right)$, we calculated $Q_d(3s3p\,^{1,3}P_{J'} - 3pnl^{1,3}L)$ as a function of n and then, using equation (9) for E_S, the sums over n for $\alpha_d(3s, 3s3p\,^{1,3}P_J)$ versus T_e.

To estimate $Q_d(j, i)$ in equation (2) for autoionizing states i with high principal quantum number n for the $3l4l'$ states (for example, for the 3s4s – 4snp dipole transitions) we used the calculated data for $n = 7$ and the $1/n^3$ scaling law for A_a and A_r as was shown above in equations (5) and 6.

The results of the calculations are shown in figure 3. In order to test the scaling, the explicitly calculated data for $n = 13$ and the scaled data for $n = 13$ derived from the calculated data for $n = 12$ were compared. It was found that the difference is within 10% that should be explained by importance of the mixing of configurations. The contributions from the scaled data are shown by curve 4 in four panels of figure 3. The values represented by this curve include the scaled data from $n = 14$ up to $n = 1000$ of the $3lnl'$ autoionizing states, from $n = 8$ up to $n = 1000$ of the $4lnl'$ states and from $n = 5$ up to $n = 1000$ of the $2p3l'3l''nl$ core-excited states. The dependence of the present results on the upper limit of n was also investigated. We found that there is a small difference for low temperature (4% for $T_e = 100$ eV) with $n = 40$ instead of $n = 1000$ as the upper limit but the difference increases for high temperatures, reaching 7% for $T_e = 1$ keV.

The high-n state contributions are very important for high temperatures. It is seen from figure 3 that for $T_e > 10$ keV, curves 4 describing the scaled contributions from the high-n states ($2p^6 3l'nl$ states with $n = 14$–1000, $4l'nl$ states with $n = 8$–1000 and $2p^5 3l'3l''nl$ states with $n = 5$–1000) are above curves 1, 2 and 3 for three panels ($2p^6 3s4s\,^3S_1$, $2p^6 3s4p\,^1P_1$, and $2p^6 3s4f\,^3F_3$ levels) shown in figure 3. The scaling contribution (curve 4) is above curves 1 and 2; however, it

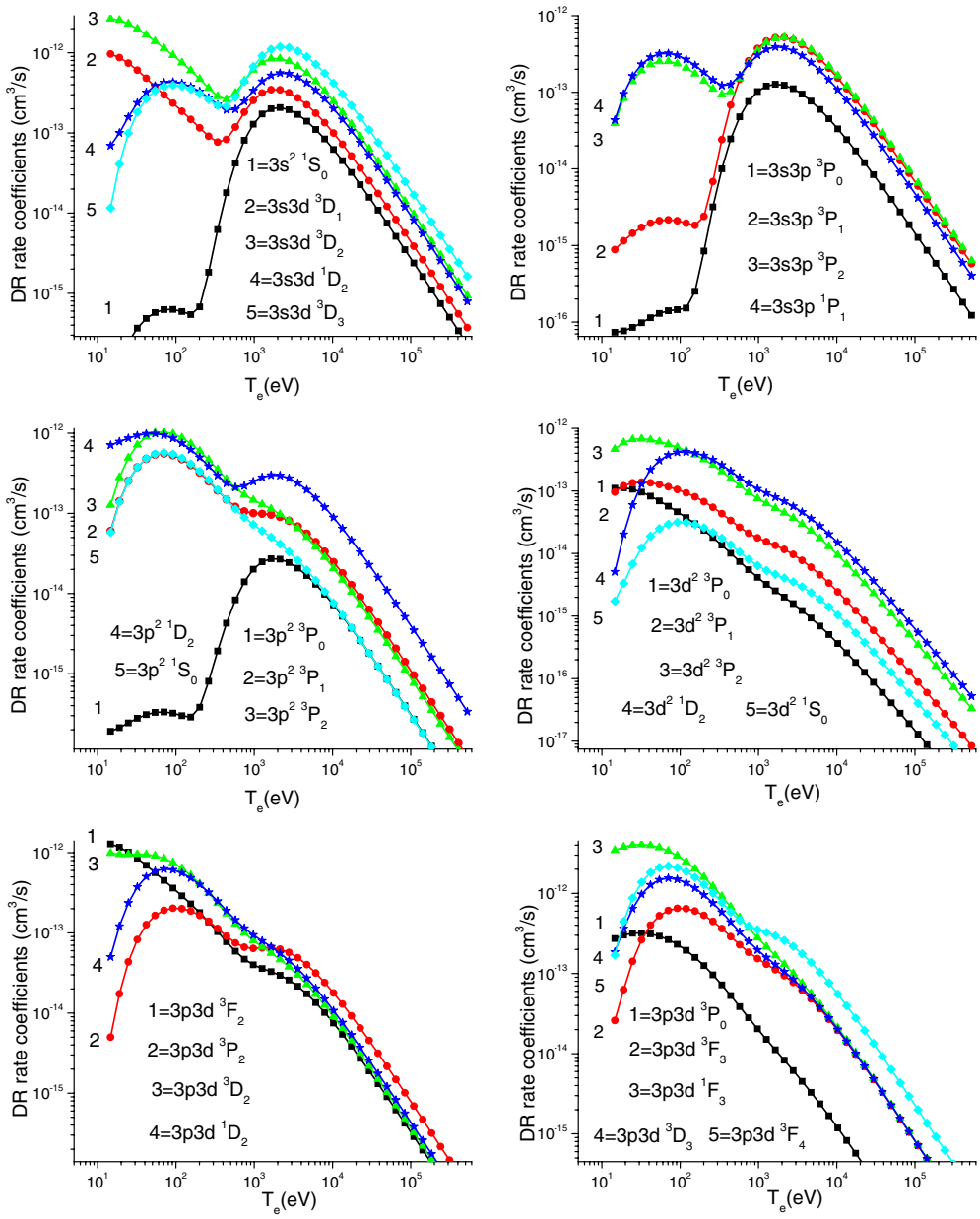

Figure 5. Dielectronic recombination rate coefficient $\alpha_d(3s, j)$ with $j = 3l3l'\,^{1,3}L_J$ as a function of T_e in Mg-like W.

is below curve 3 for the $2p^6 3s3d\,^1D_2$ level (top, left panel of figure 3). The sum of the contributions presented by curves 1, 2, 3 and 4 gives the DR rate coefficients for excited states.

In figure 4, the contribution from the $2p^6 3l'nl$, $2p^6 4l'nl$ and $2p^5 3l'3l''nl$ states to the DR rate coefficient $\sum_j \alpha_d(3s, j)$ (with j including the 35 $2p^6 3l'3l'^{,3}L_J$ and the 106 $2p^6 3l'4l'^{,3}L_J$ terms) is shown as a function of T_e in Mg-like W. Curve 4 represents the scaled contribution from the $2p^6 3l'nl$ states with $n = 14$–1000, $4l'nl$ states with $n = 8$–1000 and $2p^5 3l'3l''nl$ states with $n = 5$–1000. It is evident that the scaling contribution becomes important when the temperature T_e is larger than 100 eV. The sum of those four contributions is given by curve 5. This curve has a small maximum around 70 eV and slowly decreases (by a factor of 10 in the range from 70 eV to 6000 eV).

The calculated values of $\alpha_d(3s, j)$ are presented in figure 5 (j corresponds to $3l3l'$ states), figure 6 (j corresponds to even-parity $3l4l'$ states) and figure 7 (where j corresponds to odd-parity $3l4l'$ states). In these figures, $\alpha_d(3s, j)$ is shown for the 6 $3l3l'$ configurations and 12 $3l4l'$ configurations. The electron temperature for these plots varies from $T_e = 15$ eV to $T_e = 528$ keV. As can be seen from figures 5–7, the DR rate coefficients can be divided into three different groups based on the variation with electron temperature. There are curves without any maximum as, e.g., $\alpha_d(3s, j)$ for $j = 3d^2\,^3P_0$, $^3P_1$ (figure 5) and $3d4p\,^3D_1$ (figure 7) and the curves with two maxima (at about 70 eV and 2.0 keV), e.g., $\alpha_d(3s, j)$ for $3s3p\,^3P_2$, $^1P_1$ (figure 5). The largest group of DR rate coefficients exhibits only one maximum around 30–100 eV or 2.0–3.6 keV.

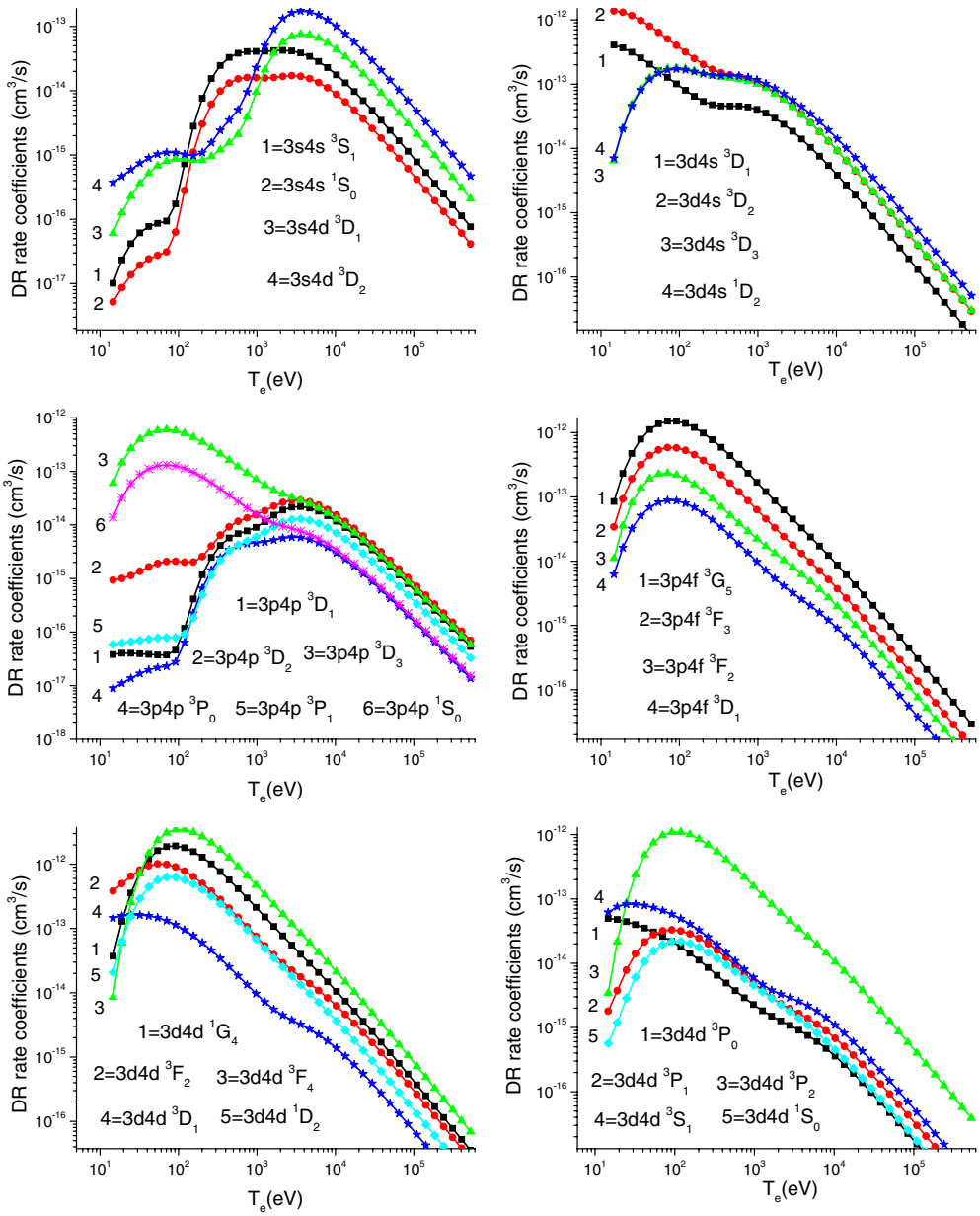

Figure 6. Dielectronic recombination rate coefficient $\alpha_d(3s, j)$ with $j = 3l4l'\,^{1,3}L_J$ (even-parity states only) as a function of T_e in Mg-like W.

5. Total dielectronic recombination rate coefficients

The total DR rate coefficients are obtained by the summation of the effective emission rate coefficients $C_S^{\rm eff}(j, i)$ (equation (3)) over all possible intermediate singly and doubly excited states:

$$\alpha_d(i_0) = \sum_i \sum_j C_S^{\rm eff}(j, i). \tag{10}$$

We have already discussed the contribution from doubly excited and core-excited states with high-n levels to the DR rate coefficients (sum over i in equation (4)). For the total DR rate coefficients one has to consider also the contribution from singly excited high-n states, i.e., the 3snl states. For these states, the most important transitions are 3snl–3pnl and 3snl–4pnl [29–31, 33, 35, 37]. Including the core-excited states creates more channels for transitions from singly excited high-n states as the 3snl–2p3s^2nl and 3snl–2p3s3dnl channels.

To estimate $Q_d(j, i)$ in equation (2) with $j = 2p^6 3snl$ and $i = 2p^6 3pnl$ for $n > 13$, we used the calculated data for $n = 12$ and the $1/n^3$ scaling law for A_a (equation (5)) and E_S (equation (9)). The values of A_r for the $2p^6 3snl$–$2p^6 3pnl$ transitions are almost independent of n since this is a one-electron 3s–3p transition. We need to take into account the change of the energy difference following equation (7):

$$A_r(3snl^{1,3}L'_{J'} - 3pnl^{1,3}L_J) = A_r(3s12l^{1,3}L'_{J'} - 3p12l^{1,3}L_J) \times \left(\frac{\Delta E(3snl^{1,3}L'_{J'} - 3pnl^{1,3}L_J)}{\Delta E(3s12l^{1,3}L'_{J'} - 3p12l^{1,3}L_J)}\right)^3. \tag{11}$$

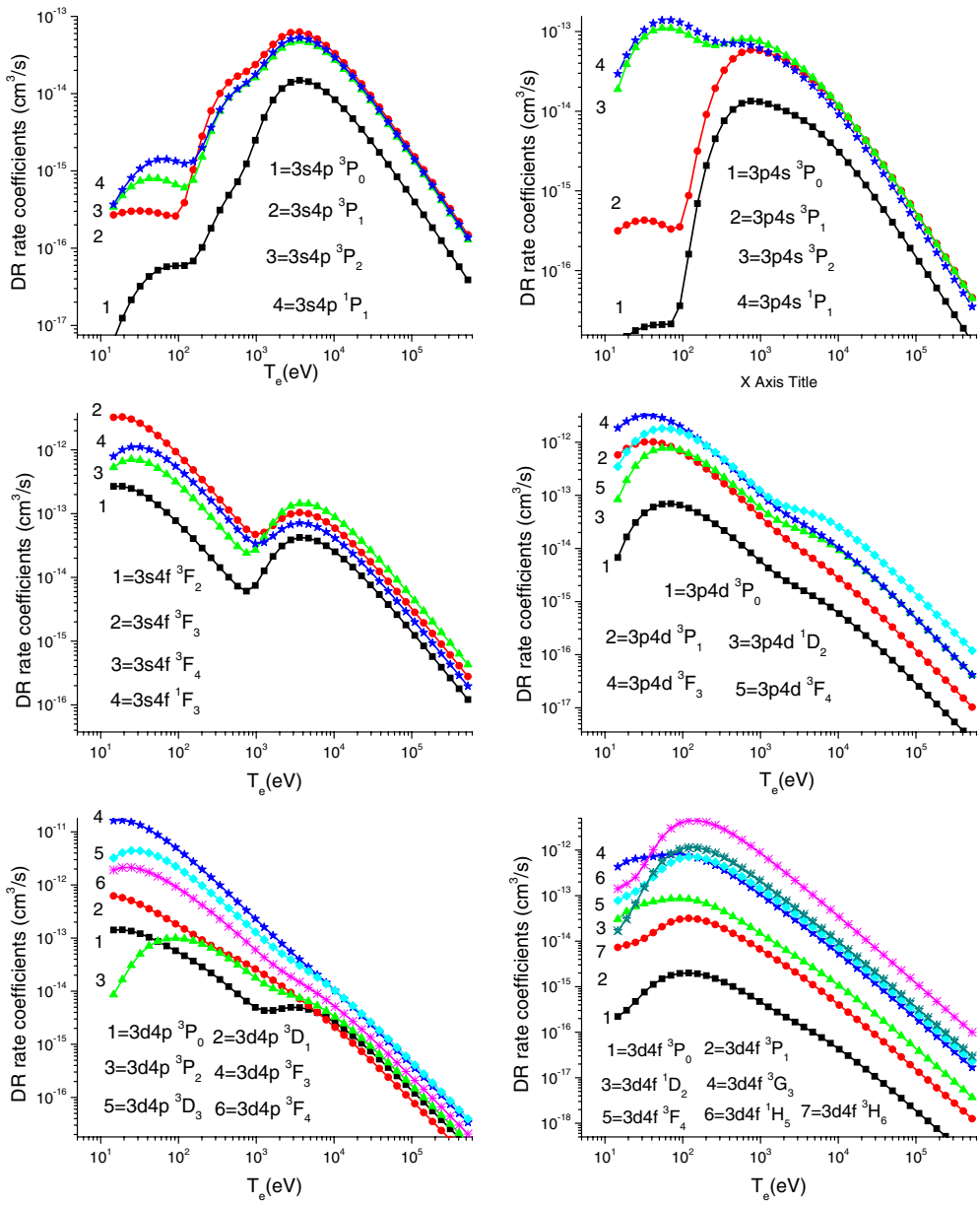

Figure 7. Dielectronic recombination rate coefficient $\alpha_d(3s, j)$ with $j = 3l4l'\,^{1,3}L_J$ (odd-parity states only) as a function of T_e in Mg-like W.

Using the asymptotic formula given by equation (8), we obtain in the first approximation:

$$\Delta E(3snl^{1,3}L'_{J'} - 3pnl^{1,3}L_J) = \Delta E(3s12l^{1,3}L'_{J'} - 3p12l^{1,3}L_J) \quad (12)$$

and finally [33]

$$A_r(3snl^{1,3}L'_{J'} - 3pnl^{1,3}L_J) = A_r(3s12l^{1,3}L'_{J'} - 3p12l^{1,3}L_J). \quad (13)$$

Again, the calculated data for $n = 12$ and the $1/n^3$ scaling law for A_a were used for estimates of $Q_d(j, i)$ in equation (2) for autoionization states i with the high values of n. For the $3snl$–$3pnl$ transitions, the scaling begins from $n = 12$. Using the scaling formulae for $A_r\left(3snl^{1,3}L'_{J'} - 3pnl^{1,3}L_J\right)$ (equation (13)) and $A_a(3pnl^{1,3}L_J)$ (equation (5)), we calculated $Q_d(3snl^{1,3}L'_{J'}$–$3pnl^{1,3}L_J)$ and then, using equation (9) for E_S, we calculated $C_S^{\rm eff}(3snl^{1,3}L'_{J'}$–$3pnl^{1,3}L_J)$. The sums over LSJ and for $C_S^{\rm eff}(3snl^{1,3}L'_{J'}$–$3pnl^{1,3}L_J)$ give data for $C_S^{\rm eff}(3snl$–$3pnl)$ as a function of nl and T_e.

The results of the calculations for $C_S^{\rm eff}(3snl$–$3pnl)$ are illustrated in figure 8 for the $2p^63snl$–$2p^63pnl$ and $2p^63snd$–$2p^63pnd$ transitions. In figure 8, we show the contribution from the scaled data for $n = 14$ to $n = 1000$ (curves 1). The contributions from the $3snl$–$4pnl$ and $2p^63snl$–$2p^53s3l'nl$ (l = s, d) transitions are shown by curves 2 and 3, respectively. We have already mentioned that the scaling for the $2p^64lnl'$ and $2p^53l'3l''nl$ states is started from $n = 8$ and $n = 5$, respectively. One can see from these plots that the largest contributions at low temperature T_e come from the $2p^63snl$–$2p^63pnl$ scaling (with a maximum value at about 300–400 eV); however, the contribution from the $2p^63snl$–$2p^53s3l'nl$ scaling is important at high T_e (the maximum value is reached at about 6.0–7.0 keV).

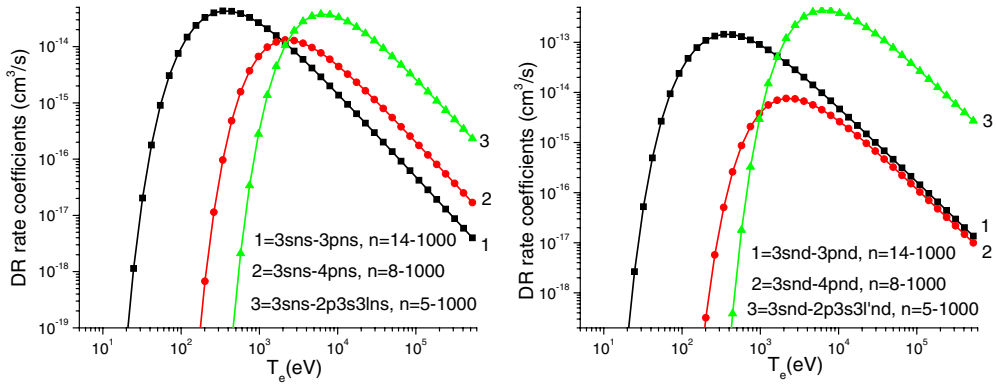

Figure 8. The $2p^63snl$–$2p^63pnl$, $2p^63snl$–$2p^64pnl$ and $2p^63snl$–$2p^53s3l'nl$ (l = s, d) contributions from the high-n states to the total DR rate coefficient $\alpha_d(3s)$ resulting from summation over i and j in equation (10).

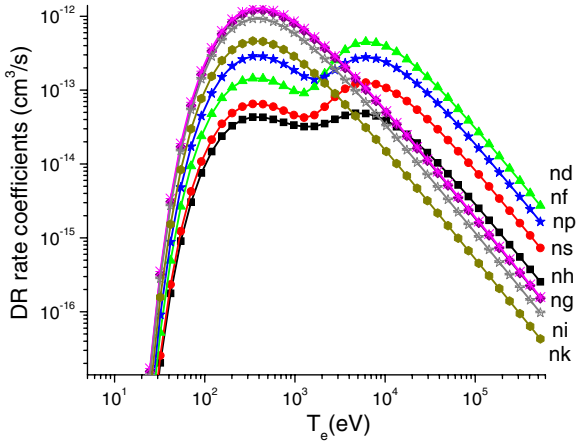

Figure 9. The sum of the [$2p^63snl$–$2p^63pnl$, $2p^63snl$–$2p^64pnl$ and $2p^63snl$–$2p^53s3l'nl$] contributions of high-n states to the total DR rate coefficient $\alpha_d(3s)$ as a function of l and T_e in Mg-like tungsten.

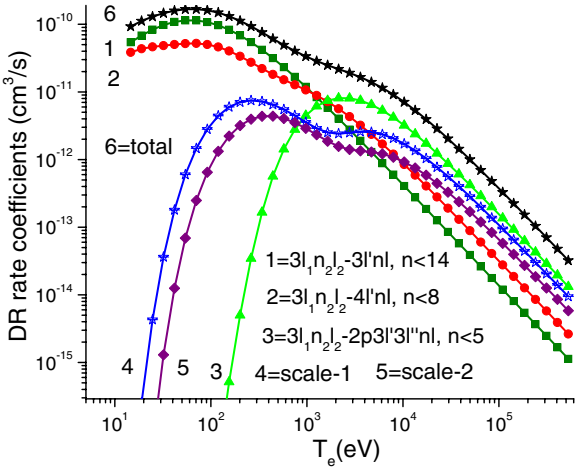

Figure 10. Total DR rate coefficient ($\alpha_d^{\rm total}$) as a function of T_e in Mg-like tungsten. 'Scale-1' describes the contribution from the high-n states for transitions from the 35 $2p^63l3l'^{\,1,3}L_J$ and the 106 $2p^63l4l''^{\,1,3}L_J$ levels to the $2p^63lnl'$ states with n = 14–1000, $2p^64lnl'$ states with n = 8–1000 and $2p^53l3l'nl_1$ states with n = 5–1000. 'Scale-2' describes the sum of the three contributions: $\sum_{n=14}^{n=1000} C_S^{\rm eff}(2p^63snl$–$2p^63pnl)$, $\sum_{n=8}^{n=1000} C_S^{\rm eff}(2p^63snl$–$2p^64pnl)$ and $\sum_{n=5}^{n=1000} C_S^{\rm eff}(2p^63snl$–$2p^53s3l'nl)$.

The final result of the sum of the $2p^63snl$–$2p^63pnl$, $2p^63snl$–$2p^64pnl$ and $2p^63snl$–$2p^53s3l'nl$ contributions from high-n states to the total DR rate coefficient $\alpha_d(3s)$ is shown in figure 9. In this figure, the values of the sum of $\sum_{n=14}^{n=1000} C_S^{\rm eff}(2p^63snl$–$2p^63pnl)$ + $\sum_{n=8}^{n=1000} C_S^{\rm eff}(2p^63snl$–$2p^64pnl)$ + $\sum_{n=5}^{n=1000} C_S^{\rm eff}(2p^63snl$–$2p^53s3l'nl)$ is presented as a function of T_e for different values of l. As can be seen from figure 9, the value of this parameter increases with increasing l up to $l = 5$ (curve 'nh'), while it becomes smaller for $l = 6$ and 7 (curves 'ni' and 'nk'). The largest contribution to the second maximum (about 6.0–7.0 keV) is obtained from values of the sum of $\sum_{n=14}^{n=1000} C_S^{\rm eff}(3snl$–$3pnl)$ + $\sum_{n=8}^{n=1000} C_S^{\rm eff}(3snl$–$4pnl)$ + $\sum_{n=5}^{n=1000} C_S^{\rm eff}(3snl$–$2p3s3l'nl)$ with $l = 2$ (curve 'nd').

The total DR rate coefficients ($\alpha_d^{\rm tot}$ in cm^3 s^{-1}) are calculated as a sum of five terms: $\alpha_d^{33}, \alpha_d^{44}, \alpha_d^{23}, \alpha_d^{\rm scale1}$ and $\alpha_d^{\rm scale2}$. The contributions of $\alpha_d^{33}, \alpha_d^{44}$ and α_d^{23} are the sums over the $2p^63l_1n_2l_2$–$2p^63l'nl$ transitions with n = 10–13, the $2p^63l_1n_2l_2$–$2p^64l'nl$ transitions with n = 4–7 and the $2p^63l_1n_2l_2$–$2p^53l'3l''nl$ transitions with n = 3–4, respectively. The parameter, $\alpha_d^{\rm scale1}$, is the contribution from the high-n states for transitions from the 35 $2p^63l3l'^{\,1,3}L_J$ and the 106 $2p^63l4l''^{\,1,3}L_J$ levels to the $2p^63l'nl$ states with n = 14–1000, $4l'nl$ states with n = 8–1000 and $2p^53l'3l''nl$ states with n = 5–1000. The parameter, $\alpha_d^{\rm scale2}$, is evaluated from the sum of three contributions: $\sum_{n=14}^{n=1000} C_S^{\rm eff}(2p^63snl$–$2p^63pnl)$, $\sum_{n=8}^{n=1000} C_S^{\rm eff}(2p^63snl$–$2p^64pnl)$ and $\sum_{n=5}^{n=1000} C_S^{\rm eff}(2p^63snl$–$2p^53s3l'nl)$.

The results for $\alpha_d^{33}, \alpha_d^{44}, \alpha_d^{23}, \alpha_d^{\rm scale1}$ and $\alpha_d^{\rm scale2}$ are shown by curves 1, 2, 3, 4 and 5 in figure 10. The electron temperature for these plots varies from 15 eV to 528 keV. It is clearly seen that the values of α_d^{33} ($2p^63l_1n_2l_2$–$2p^63l'nl$ transitions with n = 10–13) and α_d^{44} ($2p^63l_1n_2l_2$–$2p^64l'nl$ transitions with n = 4–7) represent the dominant contribution at low T_e, while the α_d^{23} term ($2p^63l_1n_2l_2$–$2p^53l'3l''nl$ transitions with n = 3–4) together with the scaled terms ($\alpha_d^{\rm scale1}$ and $\alpha_d^{\rm scale2}$) becomes more important with increasing temperature. The curves describing the contribution of the $2p^63l_1n_2l_2$–$2p^63l'nl$, $2p^63l_1n_2l_2$–$2p^64l'nl$ and $2p^63l_1n_2l_2$–$2p^53l'3l''nl$ transitions have maxima near 50 eV, 70 eV and 2.1 keV, respectively.

6. Conclusion

In the present paper, we calculated a large set of atomic data relevant to the dielectronic recombination of Na-like W into Mg-like W^{62+}.

Energy levels, wavelengths, weighted radiative transition probabilities and autoionization rates were calculated for the Mg-like tungsten ion using three theoretical methods, namely, the Hartree–Fock-relativistic method (Cowan code), the multiconfiguration relativistic Hebrew University Lawrence Livermore Atomic Code (HULLAC code) and the relativistic many-body perturbation theory method (RMBPT code) for a limited number of states. The calculated atomic data were used to obtain the dielectronic satellite lines as well as the DR rate coefficients.

We took into account the excited states $2p^6 3l'nl$ ($n = 3$–13, $l \leqslant n-1$), $2p^6 4l'nl$ ($n = 4$–7, $l \leqslant n-1$) and $2p^5 3l'3l''nl$ ($n = 3$–4, $l \leqslant n-1$) as intermediate resonance states with n up to 1000 to calculate the DR rate coefficients. Most of the state-selective DR rate coefficients reveal a double peak as a function of electron temperature. The transitions through intermediate states $2p^6 3l'nl$, $2p^6 4l'nl$ and $2p^5 3l'3l''nl$ produce a peak in the DR rate coefficients at T_e at about 50 eV, 70 eV and 2.1 kev, respectively.

The state-selective rate coefficients can be used in collisional-radiative models aimed at investigating the population kinetics in recombining plasmas as well as in calculation of ionization equilibrium. The spectra of the dielectronic satellites of W^{62+} are important in diagnostic of very high-temperature L-shell W plasmas, and of future ITER plasmas in particular.

Acknowledgments

This research was sponsored by DOE under the OFES grant DE-FG02-08ER54951 and in part under the NNSA Cooperative agreement DE-FC52-06NA27588. Work at LLNL was performed under auspices of the DOE under contract no DE-AC52-07NA2344. We would like to thank Dr A Kramida for supervising our use of his version of the COWAN code.

References

[1] Matthews G F *et al* 2007 *Phys. Scr.* T **128** 137
[2] Neu R 2006 *Phys. Scr.* T **123** 33
[3] Peacock N J, O'Mullane M G, Barnsley R and Tarbutt M R 2008 *Can. J. Phys.* **86** 277
[4] Skinner C H 2008 *Can. J. Phys.* **86** 285
[5] Loch S D, Pindzola M S, Ballance C P, Griffin D C, Whiteford A D and Pütterich T 2006 *AIP Proc.* **874** 233
[6] Clementson J, Beiersdorfer P, Gu M F, McLean H S and Wood R D 2008 *J. Phys. Conf. Ser.* **130** 001204
[7] Biedermann C, Radtke R, Seidel R and Pütterich T 2009 *Phys. Scr.* T **134** 014026
[8] Biedermann C, Radtke R, Seidel R and Behar E 2009 *J. Phys. Conf. Ser.* **163** 014023
[9] Reader J 2009 *Phys. Scr.* **134** 014023
[10] Safronova U I, Safronova A S and Beiersdorfer P 2009 *At. Data Nucl. Data Tables* at press
[11] Kramida A E and Shirai T 2009 *At. Data Nucl. Data Tables* **95** 305
[12] Beiersdorfer P, Clementson J, Gu M-F, Podpaly Y, Bitter M, Hill K W, Safronova A and Safronova U 2008 *50th Ann. Meeting APS Division of Plasma Physics* Abstract GO3.00014, http://meetings.aps.org/link/BAPS.2008.DPP.GO3-14
[13] Ralchenko Yu, Draganic I N, Tan J N, Gillaspy J D, Pomeroy J M, Reader J, Feldman U and Holland G E 2008 *J. Phys. B: At. Mol. Opt. Phys.* **41** 021003
[14] Feldman U, Seely J F, Landi E and Ralchenko Yu 2008 *Nucl. Fusion* **48** 045004
[15] Zou Yu and Froese Fischer C 2001 *J. Phys. B: At. Mol. Opt. Phys.* **34** 915
[16] Marques J P, Parente F and Indelicato P 1993 *At. Data Nucl. Data Tables* **55** 157
[17] Shorer P, Lin C D and Johnson W R 1977 *Phys. Rev.* A **16** 1109
[18] Carlson T A, Nestor C W, Wasserman N Jr and McDowell J D 1970 *At. Data Nucl. Data Tables* **2** 63
[19] Rodriges G C, Indelicato P, Santos J P, Patté P and Parente F 2004 *At. Data Nucl. Data Tables* **86** 117
[20] Cheng K-T and Johnson W R 1977 *Phys. Rev.* A **16** 263
[21] Ivanova E P, Ivanov I N and Tsirekidze M A 1986 *At. Data Nucl. Data Tables* **35** 419
[22] Safronova U I, Johnson W R and Berry H G 2000 *Phys. Rev.* A **61** 052503
[23] Safronova U I 2000 *Mol. Phys.* **98** 1213
[24] Behar E, Mandelbaum P and Schwob J L 1999 *Phys. Rev.* A **59** 2787
[25] Behar E, Peleg A, Doron R, Mandelbaum P and Schwob J L 1997 *J. Quant. Spectrosc. Radiat. Transfer* **58** 449
[26] Peleg A, Behar E, Mandelbaum P and Schwob J L 1998 *Phys. Rev.* A **57** 3493
[27] Behar E, Mandelbaum P and Schwob J L 1999 *Eur. Phys. J.* D **7** 157
[28] Meng F-C, Chen C-Y, Wang Y-S and Zou Y-M 2008 *J. Quant. Spectrosc. Radiat. Transf* **109** 2000
[29] Safronova U I, Kato T and Ohira M 1997 *J. Quant. Spectrosc. Radiat. Transfer* **58** 193
[30] Murakami I, Safronova U I and Kato T 2002 *Can. J. Phys.* **80** 1525
[31] Murakami I, Safronova U I and Kato T 1999 *J. Phys. B: At. Mol. Opt. Phys.* **32** 5351
[32] Safronova U I and Kato T 1996 *Phys. Scr.* **53** 461
[33] Kato T, Safronova U I and Ohira M 1997 *Phys. Scr.* **55** 185
[34] Murakami I, Safronova U I, Vasilyev A A and Kato T 2005 *At. Data Nucl. Data Tables* **90** 1
[35] Safronova U I and Kato T 1998 *J. Phys. B: At. Mol. Opt. Phys.* **31** 2501
[36] Safronova U I, Murakami I, Ralchenko Y, Kato T and Kato D 2006 *Phys. Scr.* **73** 143
[37] Murakami I, Kato T, Kato D, Safronova U I and Ralchenko Y 2006 *J. Phys. B: At. Mol. Opt. Phys.* **39** 1
[38] Cowan R D 1981 *The Theory of Atomic Structure and Spectra* (Berkeley: University of California Press)
[39] Bar-Shalom A, Klapisch M and Oreg J 2001 *J. Quant. Spectrsc. Radiat. Transfer* **71** 169
[40] Safronova M S, Johnson W R and Safronova U I 1996 *Phys. Rev.* A **53** 4036
[41] Safronova U I, Johnson W R, Safronova M S and Derevianko A 1999 *Phys. Scr.* **59** 286
[42] URL http://das101.isan.troitsk.ru/cowan.htm
[43] Gu M F 2008 *Can. J. Phys.* **86** 675
[44] Vainshtein L A and Safronova U I 1978 *At. Data Nucl. Data Tables* **21** 49
[45] Dubau J and Volonte S 1980 *Rep. Prog. Phys.* **43** 199
[46] Safronova U, Vasilyev A and Smith R 2000 *Can. J. Phys.* **78** 1055